



HAL
open science

Quaternary evolution of the Golo river alluvial plain (NE Corsica, France)

Stéphane Molliex, Gwenael Jouet, Pierre-henri Blard, Julien Moreau, Julie Demartini, Joep E.A. Storms, Claude Vella

► **To cite this version:**

Stéphane Molliex, Gwenael Jouet, Pierre-henri Blard, Julien Moreau, Julie Demartini, et al.. Quaternary evolution of the Golo river alluvial plain (NE Corsica, France). *Quaternary Geochronology*, 2021, 61, pp.101115. 10.1016/j.quageo.2020.101115 . hal-03053311

HAL Id: hal-03053311

<https://hal.science/hal-03053311>

Submitted on 10 Dec 2020

HAL is a multi-disciplinary open access archive for the deposit and dissemination of scientific research documents, whether they are published or not. The documents may come from teaching and research institutions in France or abroad, or from public or private research centers.

L'archive ouverte pluridisciplinaire **HAL**, est destinée au dépôt et à la diffusion de documents scientifiques de niveau recherche, publiés ou non, émanant des établissements d'enseignement et de recherche français ou étrangers, des laboratoires publics ou privés.

1 Quaternary evolution of the Golo River alluvial plain (NE Corsica, France)

2 Stéphane Molliex^{1,2*}, Gwenael Jouet³, Pierre-Henri Blard^{2,3}, Julien Moreau^{4,5}, Julie Demartini⁶, Joep E.
3 A. Storms⁷, Claude Vella⁵, ASTER Team^{5,8}

4 1- Laboratoire Geosciences Océan UMR CNRS 6538, Institut Universitaire Européen de la Mer, place N. Copernic F-29280
5 Plouzané, France.

6 2- CRPG, UMR 7358, CNRS-Université de Lorraine, 15 rue Notre Dame des Pauvres, F-54501 Vandœuvre-lès-Nancy Cedex,
7 France

8 3- Laboratoire de Glaciologie, DGES-IGEOS, Université Libre de Bruxelles, 1050 Bruxelles, Belgium

9 4- IFREMER, Département Geosciences Marines, Z.I. pointe du Diable, BP70, F-29280 Plouzané, France.

10 5- Aix-Marseille University, CNRS-IRD-Collège de France, UM34 CEREGE, BP 80, F-13545 Aix-en-Provence Cedex 4,
11 France.

12 6- ODARC, Avenue Paul Giacobbi, BP 618, F-20601 Bastia Cedex, France.

13 7- Department of Geoscience and Engineering, Delft University of Technology, Delft, The Netherlands

14 \$: Georges Aumaître, Didier L. Boulès, Karim Keddadouche.

15 *corresponding author: smolliex@gmail.com

16 KEY WORDS

17 alluvial plain; ¹⁰Be depth-profile; Quaternary; Geomorphology; Electric Resistivity Tomography; soil sequence
18 chronology; Corsica; terraces.

19 ABSTRACT

20 The Golo River drains a steep catchment (average gradient of 30 m km⁻¹, surface of 1,214 km²) in the northeast
21 part of Corsica Island, delivering sediments to the Ligurian Sea. In this study, we review and revise the geologic
22 map and constrain the extent of the Golo coastal alluvial plain formations and their relative and absolute
23 chronology. To update the surface extent of each formation, we performed a geomorphologic analysis with DEMs
24 and satellite imagery data coupled with an extensive pedogenic and sedimentary field observations database,
25 including a new borehole of 117,4 m depth. Additionally, we performed in-situ cosmogenic ¹⁰Be analysis from a
26 depth-profile in the well-preserved alluvial terrace Fy2, yielding a minimum age of 70 ka for its emplacement. Our
27 new chronology, based on cosmogenic ¹⁰Be and soil chronosequences, implies older ages than those previously
28 obtained with luminescence methods. Soil mixing by bioturbation is proposed as a possibility to explain
29 differences between luminescence and ¹⁰Be ages. In this scenario, ¹⁰Be dates the original deposition of the alluvial
30 terrace, while luminescence dates a later soil development. We highlighted at least five outcropping alluvial
31 terraces in the Golo coastal plain, which are controlled by sea-level fluctuations and were most likely deposited
32 during past sea-level highstands (close to present-day sea-level). Moreover, we identified from a borehole more
33 than 117 m of coarse fluvial sediments in the plain, that do not outcrop at the surface. New cosmogenic ²⁶Al/¹⁰Be
34 burial ages suggest that this sedimentary unit results from a thick accumulation of fluvial material filling a zone
35 significantly affected by subsidence, probably accommodated by a normal fault during the Early Quaternary.

36

37 1- INTRODUCTION

38 Coastal alluvial plains are key places for understanding sediment storage in a source-to-sink approach (e.g.
39 [Sømme et al., 2011](#); [Blum et al., 2013](#)). However, the consequences of aggradation/degradation cycles in coastal
40 plains due to Quaternary sea-level oscillations make stratigraphic correlations difficult, with upstream (alluvial
41 terraces) or downstream (shelf sediment accumulation) deposits. Since a decade, alluvial plains focused new
42 research efforts, thanks to the development of relevant tools, such as dating methods on fluvial sequences.
43 Moreover, these settings record paleo-environmental parameters controlling sediment fluxes, such as tectonics,
44 climate or sea-level fluctuations (e.g. [Twidale, 2004](#); [Allen, 2008](#)). In many cases, the extent of alluvial

45 depositional terraces in alluvial plains is mainly based on topographic constraints, such as breaks in slope and
46 escarpments (e.g. Conchon, 1975). Mapping the accurate lateral extension of alluvial terraces and determining
47 their in-depth geometry remain often problematic and suffer from large uncertainties. Notably, the relevant
48 resolution of topographic data is not always available and geophysical surveys are sometimes difficult to conduct
49 in anthropogenic areas.

50 The geochemical maturity of an alluvial soil increases with age: while Holocene deposits are not
51 weathered, soils from Pleistocene alluvial deposits of Mediterranean periglacial areas are matured, rich in clay,
52 and may become reddish after experiencing several warm phases of Quaternary climatic cycles (e.g. Baize and
53 Girard, 2008; Legros, 2012). Studying chronology of soil sequences on alluvial terraces in addition to geomorphic
54 analysis is thus a very efficient way to determine relative chronology of deposits (Hubschman, 1973; Bornand,
55 1978; Delmas et al., 2015). Moreover, the use of terrestrial cosmogenic nuclides has proven its efficiency for
56 absolute dating of alluvial deposits (e.g. Granger et al., 1995; Hancock et al., 1999; Brocard et al., 2003; Siame et
57 al., 2004; Molliex et al., 2013).

58 The high and steep topography of Corsica leads to a strong sensitivity of sediment transfers due to regional
59 climate changes, even for moderate variations (Kuhlemann et al., 2008a). The Golo River system (Eastern Corsica)
60 is considered as a reactive system (Allen, 2008), characterised by a fast sediment transfer from the catchment to
61 the sink (Sømme et al., 2011; Calvès et al., 2013; Forzoni et al., 2015), and rapidly reacts to climate changes.
62 Sediment volumes deposited in the alluvial plain and the deep-sea fan during the Holocene are compatible with
63 sedimentary fluxes inferred from cosmogenic denudation rates in the catchment (Sømme et al., 2011; Calvès et
64 al., 2013; Molliex et al., 2017). However, some studies suggest that alluvial terraces in the plain may be
65 diachronous and that the Golo River may have deposited sediment by aggradation along its entire profile at any
66 time during the late Quaternary. Such climatically-driven pulses in sediment supply may hamper detailed
67 stratigraphic correlations (Conchon, 1978; Sømme et al., 2011; Forzoni et al., 2015). The chronology of the Golo
68 alluvial terraces was first established from relative dating: Conchon (1975, 1977) associated each terrace to a full
69 glacial cycle. Later, luminescence methods applied on sand lenses of outcropping terraces (OSL on quartz and
70 IRSL on feldspar) suggested younger ages for Fy1, Fy2, Fy3 terraces, in correlation with smaller climatic
71 oscillations (Somme et al., 2011; Skyles, 2013; Forzoni et al., 2015) (Table 1). Moreover, luminescence dating
72 yields ages of terrace aggradation that are not always internally consistent, and do not always correspond to
73 climatic oscillations and full glacial stages. Sediment buffering in the alluvial and coastal plain may play an
74 important role in the transfer from the source to the sink and may alter a simple relationship between climate and
75 deposition in the alluvial plain (Somme et al., 2011; Calves et al., 2013). Obtain new absolute ages from the
76 sedimentary material of the Golo alluvial plain is thus key to progress on understanding these processes.

77 In this paper, we present an updated geological model of the Golo alluvial plain based on new data acquired
78 both in surface (geomorphology, pedology) and depth (borehole, Electrical Resistivity Tomography). We also
79 revised the chronology of formations using new cosmogenic nuclides data (^{10}Be depth profile and $^{26}\text{Al}/^{10}\text{Be}$ burial
80 ages). Finally, we discuss the Quaternary evolution of the Golo coastal alluvial plain in response to Quaternary
81 climate and tectonic forcings.

82

83 2- GEOLOGICAL SETTING

84 Corsica is an island of 8,722 km² located in the northern part of the western Mediterranean, in the Ligurian
85 Sea. It is characterized by a steep mountainous morphology, with elevations reaching more than 2,700 m (Fig.
86 1A).

87 With a catchment area of 1,214 km² and a length of 89 km, the Golo is the largest river in Corsica (Fig. 1A).
88 Originating from 1,991 m, the Golo flows mainly eastward up to the Ligurian Sea with an average gradient of 30
89 m km⁻¹ (Fig.1A). There are almost no preserved alluvial terraces in the upper part of the catchment, due to the very
90 steep and confined nature of the valleys. Despite the relatively steep slopes, there is no evidence of active or paleo-
91 landslides; all colluvial fans being covered by dense vegetation (Sømme et al., 2011). Its main tributaries are the
92 Asco (34.1 km; 165 km²), Tartagine (30.2 km; 136 km²), Casaluna (25.3 km; 100 km²), and Lagani rivers (22.1
93 km; 47 km²) (Molliex et al., 2017) (Fig.1). The Golo catchment drains two main structural domains: upstream, the
94 magmatic Hercynian domain constituted by Paleozoic crystalline rocks (granite, rhyolites, gneiss) and,
95 downstream, the metamorphic Alpine domain composed of ophiolites and low-gradient metamorphic Mesozoic
96 sediments (mainly phyllites), respectively (Fig.1B).

97 Corsica is characterised by a complex tectonic history (Mattaueer et al., 1981; Harris, 1985; Fournier et al., 1991;
98 Loÿe-Pilot et al., 2004; Fellin et al., 2006; Danisik et al., 2007). Exhumation of the inner part of the island due to
99 tectonic motions mainly occurred in the Miocene (Fellin et al., 2005a; Kuhlemann et al., 2008b). Since the late
100 Miocene, no major tectonic events have affected Corsica. However, transpressive faulting within the late Miocene
101 to Quaternary units suggest that far-field compressional stresses still affect northeastern Corsica to the present-day
102 (Fellin et al., 2005b; Serrano et al., 2013). These stresses could probably be responsible for a Plio-Quaternary
103 tilting of the alluvial plain, the adjacent coastal and shallow marine deposit (Conchon, 1975, 1978, 1999;
104 Kuhlemann et al., 2008b; Serrano et al., 2013).

105 Corsica is experiencing a subtropical Mediterranean climate with strong seasonal variability. The mean annual
106 temperature averaged over the 1981-2010 period is 15.9°C in the Golo alluvial plain (weather station of Bastia,
107 Poretta airport, 10 m above sea level, id: 20148001; (Meteo-France database;
108 https://donneespubliques.meteofrance.fr/?fond=produit&id_produit=117&id_rubrique=39)). Mean monthly
109 temperature varies between 9°C in January and 24.4°C in August. Mean precipitation is spatially variable, ranging
110 from 700 mm yr⁻¹ in the Golo alluvial plain (sea level) to 1300-1400 mm.yr⁻¹ in the highest parts of the Golo
111 catchment (~ 2,000 m) (Kuhlemann et al., 2008b; Sømme et al., 2011). Strong seasonal variations in precipitation
112 result in high variability of the river discharge: while the mean annual value is 14.8 m³.s⁻¹, the peak of discharge
113 may reach 734 m³.s⁻¹ (HYDRO French Database, www.hydro.eaufrance.fr; Valpajola station 1969-2019).
114 Vegetation is dominated by evergreen bushes and trees in the lowlands, with increasing amounts of deciduous and
115 pine forest at higher altitudes (Reille et al., 1997; 1999). There is no permanent ice present in the present-day
116 catchment area, but the uppermost part of the Golo watershed was glaciated during the Last Glacial Maximum
117 (LGM) (23-19 ka ; Mix et al., 2001) and subsequent glacial phases (Kuhlemann et al., 2005; Krumrei, 2009).
118 During the LGM, the Equilibrium-Line Altitude (ELA) varied from 1,400 to 2,000 m in the catchment, and glaciers
119 covered up to 7 % of the catchment area (Kuhlemann et al., 2005).

120 During glacial stages, Corsica was characterised by cold and dry conditions, with mean annual temperature about
121 9 °C cooler than present (Kuhlemann et al., 2005; Kuhlemann et al., 2008a; Krumrei, 2009), a 20-30% decrease of
122 mean annual precipitation (Peyron et al., 1998; Allen, 2008), even if some authors argue for a possible increase in
123 precipitation during the LGM (Kuhlemann et al., 2008a), and a herbaceous and steppe vegetation. The chronology

124 of the Late Quaternary glacier development, based on lateral moraines extent (Conchon, 1975, 1986), has recently
125 been updated by cosmogenic nuclide surface exposure dating (Kuhlemann et al., 2005; Kuhlemann et al., 2008a;
126 Krumrei, 2009).

127 Alluvial terraces of the Golo River are mainly preserved as depositional terraces in the lowland plain, between 0
128 and 100 m above present-day sea-level. This plain is only 11 km wide and consists of sediments from three alluvial
129 systems. Golo terraces constitute the main part of the alluvial plain, but alluvial deposits from two smaller coastal
130 catchments, the Bevinco to the North and Fium Alto to the South (Fig.1A) are also present. In the upper part of
131 the plain, Golo-derived alluvial deposits are sometimes mixed with locally sourced colluvial fan deposits. Alluvial
132 deposits consist of poorly-sorted, well-rounded pebbles, cobbles, and boulders supported by a clayey to sandy
133 matrix. Occasionally, well-sorted sand lenses can be found. They have been interpreted as fluvial braided channel
134 deposits (Somme et al., 2011; Forzoni et al., 2015). Bevinco and Fium Alto Rivers deposits are easily
135 distinguishable on the field, since they are exclusively constituted by Alpine domain-originated pebbles. The
136 relative age of Golo terraces have been historically based on the weathering intensity of clasts (e.g. Conchon, 1975,
137 1978). Indeed, clasts display a large range of weathering, from surface oxidation to the full destruction of the clasts
138 internal integrity (e.g. plutonic rocks such as granite, gabbro). Secondary clay content as a residual product of
139 chemical weathering has also been used for classifying and dating alluvial terraces of Golo. The characteristics of
140 each deposit (called Fz for the most recent to Fv for the oldest) of the Golo alluvial plain are synthetized in Table
141 1 (Conchon, 1975, 1978). Their relative age is currently based on correlations of moraines and weathering profiles
142 (Conchon, 1975, 1978).

143

144 **3- METHODS AND DATA**

145 *3-1 Geomorphology*

146 Since the resolution of available Digital Elevation Model (DEM) in the Golo alluvial plain was not
147 sufficient, we compiled a DEM from the digitized 1/25000-scale topographic map from the French Geographic
148 institute (IGN), complemented by a microtopographic differential GPS survey in areas of interest (e.g. alluvial
149 terraces boundaries, local depression or bulges). From this DEM, we compute gradient slope map and we extracted
150 the theoretical hydrologic network using ArcGis software[®]. In addition, satellite images (BD Ortho[®] from IGN
151 and PLEIADES[®] from the French spatial studies institute CNES), as well as field observations, were used to map
152 surface characteristics such as vegetation cover, density, degree of development of hydrologic network or flooding
153 area. Longitudinal and transversal topographic cross-sections are also performed and linked with surface soil data.

154

155 *3-2 Soil chronosequence*

156 Complete evolution of a soil overlaps several 100 ka-climatic cycles. In a sequence of Quaternary alluvial deposits,
157 different levels of soil evolution can be evidenced (Vreeken, 1975). A chronosequence of soils can thus be
158 interpreted as resulting from deposition/alteration cycles leading to the setting of successive terraces. Soils are
159 open systems that experience non-homogenous processes such as denudation and pedogenesis that may lead to
160 differences in soil formation characteristics (Durand et al., 2007). However, low-gradient alluvial plains such as
161 the Golo coastal plain undergo limited denudation (Molliex et al., 2013; Delmas et al., 2015) and are thus suitable
162 landforms for estimating soil formation rates and for assigning relative ages of alluvial deposits.

163 An extensive soil study was performed by the "Corsica's agricultural and rural development office"
164 (ODARC) (Demartini and Favreau, 2011), with 1951 auger drillings up to 1.2 m depth. The high sample density
165 (> 23 samples/km²) ensures an accurate representation of soil distribution in both alluvial plain and coastal zone.
166 The collected data include soil colour, type of material, texture or presence of leached horizons, in agreement with
167 the French updated pedologic repository (Baize and Girard, 2008) and correlated with the international Food and
168 Agricultural Organization world reference base for soil resources (FAO, 2014). Based on this extensive database,
169 we defined a classification based on petrology and clast content, texture and hydromorphic behaviour, degree of
170 weathering of parental material and different levels of soil evolution. This classification can be used as an
171 independent relative time control assuming that there is a tight relationship between the soil evolution and its age
172 (Conchon, 1975, 1978, 1980).

173

174 3-3 Electrical Resistivity Tomography

175 Electrical Resistivity Tomography (ERT) allows for imaging the electrical properties of the ground layers
176 (resistivity / conductivity). Contrasts in resistivity could be interpreted as facies differences (grain-size, clay
177 content and water content). This method is efficient to characterise alluvial deposits (Gourry et al., 2003; Crook et
178 al., 2008). Here, we used a 64 stainless electrodes Schlumberger protocol for ERT profile acquisition. We
179 sometimes elongate the profile by using rollover acquisitions (see Loke and Barker, 1996 for more details). The
180 distance between electrodes is 10 m and allows an interpretation up to a 90 m depth. In order to obtain true value
181 of depth and resistivity, we used RES2DInv software (Loke and Barker, 1996) for data inversion. The inversion
182 algorithm is based on a smoothness constrained least-squares approach (Sasaki, 1992). The Root Mean Square
183 (RMS) error gives a measure of the difference between measured and inverted models. Interpretations of ERT
184 profiles rely on a calibration realized from field observations and the local borehole database provided by the
185 "Banque de données du sous-sol" (BSS) of the French Geological Institut BRGM (<http://infoterre.brgm.fr>).

186 A survey of 53 ERT profiles has been performed in the plain, for a total of 38.5 km-length. Only two representative
187 profiles are presented in this paper. The first one is a 630 m-long East-trending ERT profile performed close to
188 Casamozza, about 80 m eastward from the basement foothills. It permitted to characterize thicknesses of different
189 alluvial deposits, which all crop out along the profile. The second one is a 950 m long N-trending ERT profile
190 aiming to constrain terraces thicknesses and geometry on both sides of the Golo River.

191

192 3-4 Borehole GBEC5-2

193 In order to improve the ground-truth stratigraphy of the Quaternary nested terraces of the alluvial plain and their
194 relationship with the bedrock, a 117.4 m-depth core borehole (GBEC 5-2) was drilled by in December 2012 by
195 the Fugro Company, using a cable drill with a diamonds crown. GBEC5-2 is located transversally to the present-
196 day Golo River, about 2 km eastward of the upper limit of the plain (9.45532°E; 42.52767°N; 18 m; WGS84). The
197 cores were first described on the field, then detailed observations were obtained in the laboratory. The recovery
198 rate is about 80% and is better at larger depths of the drilling. In order to identify differences in stacked alluvial
199 deposits, we performed a detailed petrographic study of the pebbles of the drilled material, following the pioneer
200 work of Conchon (1975; 1978) (Table 1). In practice, we identified all pebbles coarser than 4 cm and classified
201 them into 6 types of rocks, representative of the two main structural units of the Golo catchment. We identified 3
202 types of rocks for the Hercynian crystalline domain: Permian volcanism rocks (mainly rhyolites), granitoids, and

203 metamorphic basement rocks (mainly gneiss). For the Alpine domain, we defined the 3 categories: phyllites,
204 ophiolites and sedimentary rocks. A seventh marginal class is composed of rocks that do not belong to the six main
205 categories. A total of 1,252 pebbles have been identified (about 11 pebbles per meter of core). To avoid random
206 sampling bias and recuperation issues, we smoothed the results by analysing intervals of 2 m and applying a
207 running average over 3 intervals (6 m).

208

209 *3-5 ¹⁰Be - ²⁶Al cosmogenic nuclide dating*

210 In situ cosmogenic nuclides represent powerful tools to estimate the duration of a soil exposure to cosmic rays at
211 the Earth's surface (e.g. Gosse and Phillips, 2001; Dunai, 2010). Exposure durations of alluvial layers exposed to
212 denudation can be determined by the measurement of *in-situ*-produced ¹⁰Be concentrations along depth profiles
213 (e.g. Siame et al., 2004; Braucher et al., 2009; Hidy et al., 2010; Molliex et al., 2013, Saint-Carlier et al., 2016).
214 The obtained age corresponds to the end of terrace aggradation. In comparison to single dating from surface
215 samples, vertical profiles offer the opportunity to estimate both the exposure duration and the denudation rate,
216 which leads to more accurate ages (Braucher et al., 2009). The CICO profile is in the Fy2 alluvial terrace, at an
217 elevation of 5 m, far from the natural edge of the terrace. It was sampled along a recent excavation of an exploited
218 gravel pit. Eleven samples of single white quartzite or granite clasts were collected along this 4.9 m-vertical
219 section. All selected cobbles are approximately of the same size (~20 cm). For surface sample, the human-made
220 scouring of terrace surface for the gravel pit exploitation leads us to sample not directly on the profile but in the
221 nearby ground. Eight white quartzite pebbles from this surface were amalgamated and analysed for ¹⁰Be. Depths
222 of all samples in the profile were measured and corrected for the non-vertical orientation of the human-made
223 scouring. We also applied ²⁶Al/¹⁰Be burial dating on two samples from the GBEC5-2 borehole, at 37.8 m (B5S59)
224 and 116.5 m (B5S144), respectively. For these two samples, sands (250-1000 µm) from the matrix have been
225 extracted by leaching about 10 cm of a half-core.

226 Chemical treatments of samples were carried out at the "Laboratoire National des Nucléides Cosmogéniques"
227 (LN2C) at the "Centre Européen de Recherche et d'Enseignement des Géosciences de l'Environnement"
228 (CEREGE, Aix-en-Provence, France) and at PRIME lab (Purdue University, USA). First, samples were crushed
229 into a 250-1000 µm fraction. Then, they were sieved and leached several times in a mixture of HCl and H₂SiF₆,
230 up to the dissolution of all mineral fractions, except quartz. Atmospheric ¹⁰Be was removed from quartz grains by
231 3-times 40% HF successive leaching, aiming at the dissolution of 10% of quartz at each step. The cleaned quartz
232 minerals were then completely dissolved in hydrofluoric acid after addition of 100 µl of an in-house 3.10⁻³ g/g ⁹Be
233 carrier solution prepared from deep-mined phenakite (Merchel et al., 2008). Hydrofluoric and perchloric fuming
234 removed fluorides. Then, cation and anion exchange chromatography permitted to eliminate iron, manganese, and
235 other elements and obtain pure beryllium and aluminium oxides. Beryllium and Aluminium oxides were mixed to
236 a 325-mesh niobium powder prior to measurements of the ¹⁰Be/⁹Be by accelerator mass spectrometry (AMS). For
237 the samples of the terrace profile, ¹⁰Be/⁹Be ratios were measured with the "Accélérateur pour les Sciences de la
238 Terre, Environnement, Risques" (AMS-ASTER) national facility. For the borehole samples, ¹⁰Be/⁹Be ratios were
239 measured both at the AMS-ASTER and at the "Purdue Rare Isotope Measurement Laboratory (AMS-PRIME). All
240 ²⁶Al/²⁷Al ratios were measured at PRIME lab (Purdue University), as well as the ²⁷Al concentrations. The measured
241 ratios were normalized using the KNSTD07 standardization for ¹⁰Be/⁹Be (Nishiizumi et al., 2007) and KNSTD
242 standardization for ²⁶Al/²⁷Al (Nishiizumi, 2004). AMS internal counting statistics, chemical blank measurements

243 and AMS internal error (0.5%) have been taken into account to correct for analytical uncertainties (Arnold et al.,
244 2010). To obtain the most probable exposure denudation solutions for CICO profile, we used the ^{10}Be profile best-
245 fit model of Saint-Carlier et al. (2016). This Matlab© code is derived from the Hidy et al. (2010) Monte Carlo
246 model and considers the stochastic variability of the inherited component, which is the ^{10}Be concentration of the
247 detrital material before their deposition. In the modeling, we used the world averaged SLHL spallation production
248 rate of $4.13 \pm 0.20 \text{ at.g}^{-1}.\text{yr}^{-1}$ computed with the CREP calculator (<https://crep.otelo.univ-lorraine.fr/#/>, Martin et
249 al., 2017), with the Lal/Stone time dependent scaling (Stone, 2000; Balco et al., 2008), the ERA40 atmosphere
250 (Uppala et al., 2005) and the geomagnetic reconstruction of Muscheler et al., (2005). The contribution of muons
251 to the production rate was calculated using the parameters of (Braucher et al., 2011). The average density of the
252 alluvial deposit, measured from the GBEC5-2 borehole, is $2.2 \pm 0.2 \text{ g.cm}^{-3}$. We used the Chi-2 method to define the
253 best exposure-denudation solutions permitting to fit the data (Siame et al., 2004 ; Molliex et al. 2013; Saint-Carlier
254 et al., 2016) and the (Chi-2+1) domain constrains the uncertainty (Granger et al., 1996).

255 $^{26}\text{Al}/^{10}\text{Be}$ burial ages were computed assuming that, before transport and burial, the detrital material was
256 submitted to steady state denudation (e.g. Granger et al., 1996). This assumption is realistic considering the fast
257 sediment transfer due to the steep Golo River catchment morphology and the slow present-day denudation rates
258 ($\sim 0.05 \text{ mm ka}^{-1}$) (Molliex et al., 2017). Then, it is supposed that burial was rapid enough to ensure a complete and
259 definitive shielding. The Matlab© code and the parameters summarized in (Blard et al. 2019a,b) were used to
260 compute the $^{26}\text{Al}/^{10}\text{Be}$ burial ages. This approach considers that the altitude of pre-burial exposure is the mean
261 elevation of the Golo watershed, 926 m.

262

263 4- RESULTS

264 4-1 Geomorphology

265 The alluvial plain is a fairly flat eastward dipping surface characterized by a mean elevation of 36 m asl (above
266 sea level) and reaching locally 127 m asl (Fig. 2). The elevation rapidly decreases eastward (from 127 m asl to 15
267 m asl; brown to yellow in Fig. 2) from the Alpine foothills to the middle of the plain and then moderately decreases
268 from the middle of the plain to the shoreline (from 15 to 0 m asl; yellow to green in Fig. 2). Three geomorphological
269 domains in the Golo alluvial plain can be individualized from elevation and slope repartition. They are highlighted
270 by different grey tones on three longitudinal and three transversal topographic sections (Fig. 3A and 3B, location
271 of profiles in Fig. 2). From the West to the East, it corresponds respectively to the Upper, Middle and Lower Plain
272 (Fig. 3). These compartments are locally separated by main slope breaks. We defined the Upper Plain considering
273 slopes higher than $\sim 1^\circ$. They locally reach 2.7° in the northernmost part. The minimum elevation is 15 m. The
274 Middle Plain slopes range between 0.7° and 0.2° and elevation between 3 and 34 m (Fig. 3A and 3C). Lower Plain
275 slope is always lower than 0.1° and its maximal elevation is 15 m (Fig. 3A and 3C). The eastward slope gradients
276 are also imprinted by incision of the modern Golo River valley as shown by transversal profiles in each
277 morphological domain (Fig. 3B). In the Upper Plain, the Golo Valley is 130 m wide and 5 m deep (Fig. 3B profile
278 E). In the Middle Plain, the two flanks of the main Golo's channel gradually disappear seaward (Fig. 3B profile
279 F). In the Lower plain, the valley is not anymore incised (Fig. 3B, profile G).

280 Morphologically, the Upper Plain is also characterized by dendritic stream channels where second-order streams
281 are widely developed, while the Middle plain is predominantly characterized by single channel streams and a
282 sparse hydrologic network. Second-order streams are badly developed in the Lower plain. Upper and Middle plain

283 are mostly covered by oak vegetation, anthropogenic constructions or cultivated fields, while Lower Plain
284 vegetation is constituted by a mix of aquatic and shrubs swamp vegetation. Lower Plain may be flooded during
285 extreme Golo flood events. Several coastal features can also be recognised in the Lower Plain such as sandy dunes
286 and a prograding beach ridge complex with a width varying between 380 and 950 m.

287

288 *4-2 Geological mapping and soil chronosequence*

289 The type of soils in the Golo alluvial plain depends on i) the composition of pebbles in the alluvial sheets
290 on which they are developed; (ii) their degree of maturation, that depends on time. This degree of maturation can
291 thus be an efficient criterion for relative dating of alluvial terraces. We followed the nomenclature used in the
292 previous map published by the French Geological Survey Office (Lahondère et al., 1994). A synthesis of the
293 criteria used to classify terraces in function of their soil specificities is presented in Fig. 4. We summarized below
294 and in the Fig. 4 the soil and morphological characteristics of each geological unit, from the youngest to the oldest
295 and compare these characteristics with previously published ages and terrace nomenclature (Table 1). The
296 classification of Golo alluvial plain deposits resulted in the definition of 8 soils, including 6 which could be related
297 to alluvial deposits. Fig. 5 displays the revised geological map of the Golo alluvial plain, based on soil
298 chronosequences and morphological analysis.

299 Modern deposits are Mz, Fz and Fzl. (i) Mz is the littoral fringe, it is composed of a unit of prograding
300 sandy beach ridges that could extend up to 950 m inland. Soil is not developed, and only sparse vegetation is
301 present on these sandy beach ridges. (ii) Fz represents the present-day alluvial deposits, characterized by a Raw
302 Fluvisol, a term used for the surface of modern active streams deposits (FAO, 2014). The formation is constituted
303 either by gravelly-sandy braidplain deposits and finer grained (sand) palaeo-meanders (mainly to the east) and lies
304 in the active bed of the Golo River (Fig. 5). Pebbles and cobbles are fresh and there is no clue of any soil horizons.
305 (iii) Fzl corresponds to fine-grained (silt) sediments which are interpreted as modern floodplain deposits which
306 overlies older alluvial terraces (Sømme et al., 2011). It is located in the lower plain (Fig. 5). The lateral extent of
307 this unit is associated with considerable uncertainty because it is deduced from a compilation of isolated
308 observations (mechanic soundings, boreholes or field observations during or after flooding events; Demartini and
309 Favreau, 2011).

310 Fy3 alluvial formations are characterized by the development of Typical Fluvisols, a mix of pebbles and sands in
311 surface, with a beginning of soil formation, with weak horizon differentiation. Pebbles and cobbles are weakly
312 weathered. Sometime a beginning of decarbonation may occur (Fig. 4). Fy3 typically constitutes the flood bed of
313 almost all rivers through the plain.

314 Fy2 alluvial formations are characterized by the development of Brunisols, characterized by a brownish colour,
315 composed by three horizons and moderately developed in depth (about 20 cm). Granite and phyllites elements are
316 weathered and contribute to the development of a thin brown clay-rich horizon. These soils are leached, but not
317 heavily, a differential weathering that led to the formation of Al and Fe oxides, responsible for the overall brown
318 colour (Fig. 5). Fy2 is mostly located to the North of the present-day Golo River (98 %). It extends from the
319 basement foothills to the middle plain (Fig. 5) and present an average slope of $\sim 0.2^\circ$ toward the sea (Fig. 3).

320 Fy1 alluvial formations are characterized by the development of Reddish Brunisols, characterized by a well-
321 developed leached surface horizon, a thickness comprised between 10 and 50 cm and yellow to red colours (Fig.
322 4). They are mainly preserved in the middle (61.5 %) and the upper plain (30.5 %). Fy1 present a mean slope

323 ranging from $\sim 0.3^\circ$ to the South to $\sim 0.7^\circ$ to the North (Fig. 3). Fy1 could also be differentiated from Fy2 because
324 of well-developed scarps of several meters between Fy1 (above) and Fy2 (below) (Fig. 5). Based on the arguments
325 discussed for Fy2 chronostratigraphy, this sequence should represent older interglacial alluvial sediments.
326 Fx alluvial formations are characterized by the development of Luvisols characterized by an extensively leached
327 layer in surface that is nearly free of clay and iron-bearing minerals. A layer of mixed clay accumulation lies
328 below, with high concentrations in available ions. Surface leached horizons are more and more developed with
329 soil maturity (up to 5 horizons) and may exceed several meters in the most evolved soils (Fig. 4). These deposits
330 are mainly located in the upper plain (97 %). Field observations (outcrops and soils) suggest that Fx is only related
331 to minor rivers in the plain (Pietre Turchine, Rasignani, Fig. 5), outside of the Golo catchment area, since it is
332 constituted only by Alpine domain-derived sediment. We did not observe Fx surface deposits that originated from
333 the Golo Catchment, in contrast to previous interpretations (Conchon, 1975, 1978).
334 Fw is presumably the oldest formation that crops out in the plain. It is characterized by the development of
335 Ferralsols with diffuse horizon boundaries, a clay- and iron oxides- rich horizon mainly composed of kaolinite that
336 can reach a thickness of 1m (Fig. 4). All pebbles and cobbles are affected by such weathering that some of them
337 are entirely destroyed. Some resistant pebbles and cobbles (rhyolite) present a 3-4 cm ring of weathering. Primary
338 clay derived from degradation of clasts feeds into the deeper clay-rich horizon. Fw lies almost exclusively in the
339 upper Plain. Only a small area located to the South of the present-day Golo River presents a combined Hercynian-
340 Alpine provenance clasts assemblage, which is the signature of a Golo River provenance (Fig. 5). The high slope
341 gradient of the Fw surface ($> 1^\circ$) results in a truncated soil profile with absence of leached horizons. The
342 downstream limit of the Fw terrace is almost always marked by abrupt slope changes from higher to lower slope
343 values (Figs. 2, 3 and 5).

344

345 *4-3 Electrical Resistivity Tomography*

346 A 630 m-long East-trending ERT profile was performed close to Casamozza. From the results and the mapping of
347 the terraces, three electrical units corresponding to Fy3, Fy2 and Fy1 terraces can be distinguished in the 630 m-
348 long East-trending ERT profile, about 80 m eastward from the basement foothills (Fig. 6A, location in Fig. 5).
349 These units present relative resistivities which slightly decrease with age, with values of 400-800 ohms.m⁻¹, 300-
350 600 ohms.m⁻¹ and 240-500 ohms.m⁻¹, for Fy3, Fy2 and Fy1, respectively. Resistivity values for Fw are lower
351 westward, ranging from 80 to 280 ohm.m⁻¹. At depth, resistivity values range from 20 to 80 ohms.m⁻¹, and likely
352 represent a formation that does not crop out at the surface (see part 5.2 for discussion). The mean thicknesses of
353 Fy3, Fy2, Fy1 are 10 to 15 m while mean thickness of Fw is more likely to be 20 m (Fig. 6A). Note that resistivity
354 values are locally scattered due to terrace heterogeneities and/or differences in the conductivity of the groundwater.
355 Relative resistivity values for Fz, Fy3, and Fy2 terraces in the N-trending ERT profile (Fig. 6B, location in Fig. 5)
356 are about 120-250 ohms.m⁻¹, 300-800 ohms.m⁻¹ and 700-800 ohms.m⁻¹, respectively (Fig. 6B). The differences of
357 resistivity between the two profiles may be explained by soil water content and/or the heterogeneity of alluvial
358 material in relation with the main Golo riverbed distance. A staircase contact is evidenced between Fy3 and Fy2,
359 consistent with a topographic escarpment of approximately 5 m between the two units (Fig. 3; Fig.6B). A similar
360 contact is presumed between the less resistive Fz terrace and the Fy3 terrace. The topographic bulges on both sides
361 of the Golo River consist of human-made dams. The Fy2, Fy3 and Fz alluvial terraces overlie a heterogeneous
362 succession with two stacked layers, a 180-500 ohms.m⁻¹ unit, which overlies a 10-80 ohms.m⁻¹ unit. Accordingly

363 to GBEC5-2 borehole and field data (cf. Part 4.4), the 180-500 ohms.m⁻¹ unit may correspond to Fw terrace, while
364 the 10-80 ohms.m⁻¹ unit corresponds to an alluvial sheet not known from the surface (see part 5.2 for discussion).
365 The high resistivity anomaly observed around 90 m depth (Fig. 6B) is possibly an artefact or a local heterogeneity
366 or change in water chemistry, since no change in facies was noticed in the borehole GBEC5-2, that was drilled
367 after the ERT profile (Fig. 7).

368

369 *4-4 Borehole data*

370 The GBEC5-2 borehole shows a very homogenous 117.4 m of continental alluvial sand and gravel deposits in a
371 clay-dominated matrix (Fig. 7). Marine strata were not deposited and/or preserved in the stratigraphic column. The
372 bedrock was not reached. [Conchon \(1975, 1977\)](#) had already suggested a thick (at least 150 m) stacked braided
373 alluvial sequence underneath the Golo alluvial plain, based on geophysical data (vertical electrical sounding).

374 There is no sharp transitions in the recovered cores, except within the first 20 m, where two paleosoils are identified
375 by a reddish coloration of the matrix and a complete disaggregation of the clasts. These two reddish levels are at
376 8.5 and 18.5 m depth, respectively (Fig. 7A). By analogy with the correlation previously made between alluvial
377 formation and their soil evolution, these levels can be interpreted as paleosoils of terraces older than Fy2. Terrace
378 mapping and ERT data suggest that the surface is constituted by Fy3 terrace directly lying on Fy1; Fy2 has been
379 entirely removed by Fy3 erosion. The first reddish level can thus correspond to the top of Fy1 terrace at 8.5 m. In
380 the Golo alluvial plain, Fx is not recognized at surface and Fy1 is often in direct contact with Fw. The second
381 reddish level could thus be interpreted as the limit between Fw and Fy1, at 18.5 m depth (Fig. 7A). The top of an
382 aquifer layer was crossed at 39.5 m depth during drilling (Fig. 7A). It could correspond to a transition between a
383 permeable (above) and an impermeable (below) layer, even if no clear facies change is noticed. Petrologic analyses
384 do not allow for an accurate differentiation of terraces in function of clast petrography. However, it is possible to
385 note that, at about 40 m, pebbles are more weathered, with a drastic decrease of the recovery of pebbles (Fig. 7B).
386 Moreover, granitoids and phyllites are less abundant than rhyolites and ophiolites, which are the more resistant
387 rocks in the catchment ([Molliex et al., 2017](#)). If the presence of water may increase the weathering, other causes
388 also have to be considered. Indeed, why water could circulate here and nowhere else? We thus suggest that, at 40
389 m, this weathered level results in the presence of a paleo-aquifer. This weathered level was probably exposed
390 sufficiently long enough at the surface for removing a large part of soft rocks by erosion. From this depth,
391 composition of pebbles progressively evolved, up to about 60 m depth. Indeed, in the first ~40 m, pebbles from
392 the Hercynian domain represent about 55 % of the total pebbles, and Alpine phyllites pebbles about 10 %. Below
393 60 m, the content of Alpine phyllites pebbles is much higher (30 % of total pebbles), while Hercynian domain
394 pebbles are represented less frequently (only 40 % of the total pebbles). The zone between 40 m and 60 m depth
395 can be considered as a transition zone between the two petrologic compositions. No paleosoils nor evidence of any
396 other transition can be identified over the 60-117.4 m core section (Fig. 7A).

397

398 *4-5 Cosmogenic ¹⁰Be and ²⁶Al data*

399 ¹⁰Be concentrations measured in the CICO vertical depth profile (Fy2 terrace) are compatible with a near
400 exponential decrease with depth (Fig. 8B and Table 2). This indicates that: i) the analysed samples remained in
401 their relative and sampled positions since the terrace deposition and, therefore, that the build-up of in-situ
402 cosmogenic ¹⁰Be in this sedimentary material most probably occurred after one single deposition event, ii) the

403 dispersion due to variable pre-exposure is not significant compared to the age of the terrace exposure. The higher
404 concentrations in CICO 70 and CICO 200 samples probably result from a complex pre-deposition exposure history
405 in the upper catchment. The inverse modeling of this profile did not permit to define only one single "denudation
406 - exposure duration" scenario, indicating that the terrace reached what is called steady-state denudation. In this
407 case, the production of ^{10}Be is balanced by the loss due to the surface denudation (Fig. 8). Such configuration only
408 permits to derive a minimum exposure age, a denudation rate and the value of the pre-deposition concentration.
409 The obtained best-fit scenario indicates with a high level of confidence that: i) the exposure duration of terrace
410 Fy2 is at least 70 ka, ii) the surface denudation rate of Fy2 is $10 \pm 2 \text{ mm.k.a}^{-1}$ and iii) the mean inherited ^{10}Be of
411 the Fy2 silico-clastic material is $6 \times 10^4 \text{ at.g (SiO}_2\text{)}^{-1}$ (Fig. 8B). This value can also be used to calculate a paleo-
412 denudation rate at the time of terrace deposition: $95 \pm 4 \text{ mm.k.a}^{-1}$.

413 The $^{26}\text{Al}/^{10}\text{Be}$ burial ages from the GBEC5-2 borehole are $2.45 \pm 0.73 \text{ Ma}$ at 37.8 m (sample B5S59) and 2.74
414 $\pm 0.95 \text{ Ma}$ at 116.5 m (sample B5S144), respectively (Table 3).

415

416 5- DISCUSSION

417 5-1 Chronology of Late Pleistocene events

418 Aggradation of sediment in alluvial systems depends of slope, base level and sediment transport rate (e.g.
419 Blum and Törnqvist, 2000). In a coastal alluvial plain such as the Golo, fluvial aggradation is strongly controlled
420 by sea-level fluctuations. Fluvial aggradation generally occurs during sea-level highstands, i.e. deglacial (valley
421 filling) and interglacial (upstream overflow) stages (e.g. Blum and Törnqvist, 2000), because fluvial slope may
422 decrease, as well as the transport capacity of sediments. Lowstand alluvial units were deposited on the middle and
423 outer shelf (Sweet et al., 2020). Nevertheless, aggradation in the plain may also occur during glacial stages if
424 sediment supply overloads the channel transport capacity (e.g. Blum and Törnqvist, 2000; Forzoni et al., 2015). In
425 Mediterranean regions, sapropel events are recognized as markers of an increase of freshwater runoff during
426 interglacial stages (Rohling et al., 1991; 2015; Milner et al., 2012, Toucanne et al., 2015) and suggest that sediment
427 supply during glacial and interglacial periods are not very different in average, despite glacial periods are generally
428 recognized to trigger larger input (Kettner and Syvitsky, 2009). Numerical modeling however suggests that the
429 sediment supply during MIS4 and MIS2 was twice the one of the Holocene (Forzoni et al., 2015). In our following
430 interpretations, we therefore consider that aggradation of alluvial material in the present-day emerged Golo coastal
431 plain occurred during sea-level rise, i.e. from deglacial to interglacial stages. This interpretation is supported by
432 the luminescence and ^{14}C dating of the most recent unit (Fy3) of the Golo plain (Sømme et al., 2011; Forzoni et
433 al., 2015) and also by the presence of a past sea-level highstand beach sand level into the terrace Fy1 in the Sagone
434 Gulf (SW Corsica) (Conchon, 1989).

435 Based on the new cosmogenic ^{10}Be CICO profile dating of Fy2 and relative pedologic observations, we
436 revisit the chronology of the Golo alluvial plain deposits. Old and new chronologies are summarized in Table 1.
437 After the end of the Last Glacial Maximum, during the deglaciation (i.e. $\sim 10\text{-}15 \text{ ka}$), Fy3 alluvial sheet was
438 deposited in response to sea-level rise and the increased discharge of sediment supply triggered by glaciers melting
439 in the upper catchment, as demonstrated by hydro-sedimentary simulations (Forzoni et al., 2015), that filled the
440 incised hydrographic network developed during the MIS2 glacial stage. The sediment supply then decreased
441 during the Holocene, leading to a change in fluvial style, from braided (Fz) to meandering (Fzl) deposits (e.g.
442 Blum and Törnqvist, 2000). Fzl deposits are dated by OSL at $3.18 \pm 0.98 \text{ ka}$ (Skyles, 2013).

443 Forzoni et al. (2015) suggest elevated temperature post-IR IRSL (pIRIR₂₉₀) ages for Fy2 terrace of $43 \pm$
444 4 and 46 ± 7 ka (Fig. 5; Table 4). They associated this deposit to the warming at the onset of MIS 3. Our new in
445 situ cosmogenic ¹⁰Be profile in the same terrace yields a minimum abandonment age of 70 ka (at least MIS5a),
446 older than these luminescence ages. Even if some studies suggested the possibility of overestimated ages in ¹⁰Be
447 concentration depth profile measurements resulting from heterogeneous residual inheritance in pebbles (Le Dortz
448 et al., 2012), the ¹⁰Be CICO profile analysed displays a near perfect exponential decrease with depth (Fig. 8B) and
449 our modelling approach takes into account the impact of inheritance on the exposure duration (Saint-Carlier et al.,
450 2016). On the contrary, our inverse modelling shows that the ¹⁰Be CICO profile mandates a minimum deposition
451 age of 70 ka (at least transition MIS 5 / MIS 4) (Fig. 8B). In > 70 ka offshore Golo deposits, Sweet et al. (2020)
452 also identified quartz OSL luminescence ages younger than the deposition ages based on the $\delta^{18}\text{O}$ chronology. The
453 fact that luminescence ages for sediment older than 70 ka may be underestimated in some context is still a debated
454 topic that may involve several mechanisms, such as the saturation of the thermal signal in quartz (e.g. Steffen et
455 al., 2009; Lowick and Preusser, 2011; Lowick and Valla, 2018) and the grain size dependence of the signal (e.g.
456 Buylaert et al., 2007; Timar et al., 2010; Fan et al., 2010; Timar-Gabor et al., 2017). Forzoni et al. (2015) were
457 aware of these potential limitations and thus applied IRSL on feldspars, instead of quartz. For IRSL, the anomalous
458 fading in feldspars may also lead to a possible age underestimate (e.g. Wintle, 1973; Auclair et al. 2003; 2007;
459 Kars et al., 2008; Li et al., 2018). Forzoni et al. 2015 applied pIRIR₂₉₀ feldspar dating to overcome problems related
460 to early signal saturation (quartz OSL) and anomalous fading (conventional IRSL feldspar dating) (e.g. Li and Li,
461 2011; Thiel et al., 2011; Buylaert et al., 2012, Kars et al. 2012). Thus, age disagreement can neither be explained
462 by too early saturation, nor by fading. Another bias could arise from the water content estimation, which may
463 overestimate the environmental dose rates and thus underestimate luminescence ages (e.g. Duller, 1994; Jeong et
464 al., 2007; Carr et al., 2019). Indeed, constraining the exact water content for the entire burial period is not a
465 straightforward task. However, even if the wettest possible scenario is considered for these deposits, IRSL age
466 would only increase by ~10%, i.e. from ~45 ka to ~49 ka, which is not enough to explain the observed age
467 difference. Another cause for the ¹⁰Be-luminescence discrepancy could be the use of contrasted grain size: ¹⁰Be
468 analyses were performed in pluri-centimetric quartz cobbles, while pIRIR₂₉₀ in sand-sized (200-250 μm) feldspars.
469 The sand fraction is sensitive to biological soil mixing, which can be highly effective in exposing grains at the
470 surface, thus resetting the pIRIR₂₉₀ signal (Reimann et al., 2017). The CICO pIRIR₂₉₀ samples are at about 2 m
471 depth and deep-rooted vegetation reach the sandy layer dated by pIRIR₂₉₀ (Fig. 9A), also implying modifications
472 of fluids circulation into the sand layer. Thus, we could reasonably suggest that the luminescence ages for Fy2
473 have been rejuvenated by these hydro-biological processes. If correct, this scenario suggests that ¹⁰Be dates the
474 original deposition of the alluvial terrace, while luminescence dates the later soil development.

475 An interesting and complementary observation lies in the sea level, which was 40-70 m below the present-
476 day level during MIS3 (~25-60 ka) (Spratt and Lisiecki, 2016). At this time, the depocenters were located offshore
477 of the current alluvial plain (Sweet et al., 2020), aggradation in the plain was thus very unlikely or limited, while
478 such conditions were favourable to a soil development on Fy2. Based on the cosmogenic ¹⁰Be profile (that yields
479 a minimum terrace exposition of 70 ka), relative pedologic observations and comparisons with alluvial regional
480 deposits, we propose that the emplacement of the Fy2 terrace occurred during one of the highest sea-level of MIS
481 5 (5a, ~82 ka) (or during 5c, 5e, or a composite of all these MIS 5 high sea-level stages). Then, the abandonment
482 age of Fy2 was probably around 70 ka, just after the MIS 5a-4 cooling. This climatic transition very often led to

483 the abandonment of geomorphological surfaces in coastal environments worldwide (e.g., [Pedoja et al., 2011](#)),
484 consistently with the chronology of sea-level fluctuations: MIS 5a was indeed the last sea level highstand before
485 the Holocene ([Spratt and Lisiecki, 2016](#)). This interpretation would also be consistent with the presence of a
486 Brunisol developed above Fy2, under the cold and dry conditions of MIS 4 to MIS 2 that are not favorable to Fe
487 oxidation. Moreover, alluvial deposits similar in age and soil facies and under a similar Mediterranean climate are
488 widely preserved in Southern France ([Brocard et al., 2003](#); [Siame et al., 2004](#); [Molliex et al., 2013](#), [Delmas et al.,](#)
489 [2018](#)).

490 For Fy1, IRSL analyses on feldspar yield pIRIR₂₉₀ ages of 92 ± 11 ka and 100 ± 12 ka ([Forzoni et al.,](#)
491 [2015](#)) (Fig. 5, Table 4). At that site, there is no evidence of biological perturbations at the IRSL sample level (~4
492 m depth) (Fig. 9B). If these pIRIR₂₉₀ ages are representative of the deposition age of Fy1, this terrace would have
493 been deposited during MIS 5c. However, the soil developed on Fy1 is widely oxidized (Reddish Brunisol). Fy1 is
494 the youngest reddish terrace, with a soil that is still partially brown, i.e. has not been entirely oxidized. This likely
495 indicates that this terrace experienced just one warm climatic optimum after its deposition. The youngest
496 interglacial stage able to create reddish soils is the Eemian period, MIS 5e, between 124 and 119 ka ([Legros, 2012](#);
497 [Delmas et al., 2015](#); [Hughes and Gibbard, 2018](#)), because it is the warmest and the wettest one. Deposition of Fy1
498 would thus be not much older than MIS 5. Since terraces in the alluvial plain are deposited during highstands, the
499 deposition of Fy1 may have occurred during the MIS 7 to MIS 6 transition (190 ka; [Spratt and Lisiecki, 2016](#);
500 [Hughes and Gibbard, 2018](#)). This age would be consistent with the dating of a regional well-preserved terrace
501 level in southern France ([Brocard et al. 2003](#); [Molliex et al., 2013](#), [Delmas et al., 2018](#)). However, an MIS 5c age
502 for Fy1, with a reddish soil development during the MIS 5a cannot be totally excluded.

503 Fx is not present at the surface of the Golo River alluvial plain. Its deposition could correspond to the MIS 10-
504 MIS 11 transition (about 400 ka), because MIS11 is known as one of the warmest interglacial with a high sea-level
505 ([Spratt and Lisiecki, 2016](#); [Hughes and Gibbard, 2018](#)).

506 Two quartz OSL ages for the Fw terrace are reported by [Somme et al \(2011\)](#). They are 44 ± 3 and 61 ± 4 ka (Fig.
507 5, Table 4). These ages are clearly too young, the samples most likely suffered from quartz saturation as reported
508 by [Forzoni et al \(2015\)](#) and should therefore not be considered. The characteristics of soils developed on this
509 terrace suggest that it experienced at least the last interglacial period (i.e. MIS 5e; 120 ka) ([Pedro, 1968](#); [Demartini](#)
510 [and Favreau, 2011](#); [Legros, 2012](#)), like Fy1. No more accurate age constraints are available for Fw. We suggest
511 that Fw was probably deposited during the warm interglacials that occurred between MIS 19 and MIS 23; about
512 800-1000 ka), since this stage corresponds to the first of the 100-ka climatic cycles since the middle Pleistocene
513 transition; ~0.9 Ma) and is probably one of the best preserved level for Early Quaternary terraces in Southern
514 France ([Colomb et Roux, 1978](#); [Dubar, 1984](#); [Delmas et al., 2018](#)).

515 At lower depth, samples from the borehole GBEC5-2 yield similar $^{26}\text{Al}/^{10}\text{Be}$ burial durations of $2.45 \pm$
516 0.73 Ma at 37.8 m and 2.74 ± 0.95 Ma at 116.5 m in (Table 3). These data indicate that the unknown thick formation
517 evidenced from ~40 to 117 m in the GBEC5 borehole, that is stratigraphically older than the Fw terrace, likely
518 results from accumulation of sediments during the end of the Pliocene or the beginning of the Quaternary, around
519 2.6 Ma. Despite large uncertainties, these ages suggest that the accumulation rate of sediments was high during
520 this period, implying a rapid infilling of an accumulation space.

521

522 *5-2 Geodynamic evolution of the Golo alluvial plain*

523 The presence of more than 117 m of continental Quaternary alluvial deposits evidenced in the GBEC5-2 borehole
524 is enigmatic (Fig. 10A; 10B; 10D). Indeed, during the Quaternary, the climatic oscillations lead to strong sea-level
525 variations (up to 120 m), and thus rapid aggradation/degradation cycles in the alluvial plain, with the onset of
526 alluvial terraces in the plain during the highstands and their destruction by incision and erosion during lowstands.
527 In this context (subsidence and sea-level drops and rises), marine deposits should have been preserved in a borehole
528 crossing a 0-100 m range of elevation below the sea level. The sea-level have oscillated only between 50 and -50
529 m during the Early Pleistocene (Miller et al., 2005; de Boer et al., 2010; Rohling et al., 2014). The base of the
530 GBEC5-2 borehole (at least from -67 m depth) should thus be constituted by marine deposits, even during
531 lowstands. As there are no marine sediments preserved in the borehole, we can postulate than subsidence occurred
532 in the alluvial plain at least since the Plio-Pleistocene transition, 2.6 Ma. Considering the location of the borehole
533 and the chronology of the deposits, subsidence of the Golo River alluvial plain should be invoked to explain a
534 continental infilling. However, the high slope of the old Quaternary terraces and the cut-and-fill geometry of these
535 terraces only 1-km upstream also argue for a long-term uplift of the upstream part of the catchment, in agreement
536 with post-Miocene exhumation of the inner part of Corsica (Fellin et al., 2005a). Given the short distance between
537 these two domains, a tilting of the margin is unlikely to occur. A control by a fault delimiting the eastern subsiding
538 plain and the western highlands is more plausible. Such fault would have accommodated at least 77 m of vertical
539 motion during the whole Quaternary (Fig. 10C). This fault would correspond to the sharp contact between the
540 bedrock and the Quaternary formations, at the western margin of the Golo alluvial plain. There is only sparse
541 evidence of recent tectonic activity documented in Corsica (e.g. Conchon, 1977, 1999; Fellin et al., 2005a; Serrano
542 et al., 2013). No active structure is referenced yet in Corsica and instrumental and historical seismicity is very low
543 (SISFRANCE database). The estimated subsidence rate should be at least 77 m in ~ 2.6 Ma, i.e. ~ 0.03 mm yr⁻¹,
544 consistent with mean deformation rates of active regional tectonic structures in Southern France (0.02-0.01 mm
545 yr⁻¹ after Molliex, 2009). The apparent sedimentation rate at the bottom of the borehole is high (~77 m in 0.4 Ma,
546 ~ 0.2 mm yr⁻¹). A part of this accumulation might be due to the infilling of a paleo-valley. However, given
547 uncertainties on ²⁶Al/¹⁰Be ages (2.45 ± 0.73 and 2.74 ± 0.95 Ma; Table 3) such rates must be considered with
548 caution.

549 Because of the absence of marine deposits in the borehole deposits, and without evidence of drastic
550 change in sediment supply, we can postulate that the alluvial plain was already filled by continental sediment
551 before the onset of the large eustatic oscillations (~120 m) after the Mid-Pleistocene transition (0.9 Ma; e.g.
552 Gibbard et al., 2010). The onset of the 100 ka glacial cycles after the Mid-Pleistocene transition have probably
553 increased exhumation and denudation rates (Champagnac et al., 2007; Valla et al., 2011; Hermann et al., 2013).
554 In the Inner Alps the exhumation and denudation of crystalline rocks was enhanced, as evidenced by an increase
555 of the proportion of crystalline rocks among the sediments deposited in the Inner Alps forelands (Petit et al., 1996;
556 Boenigk and Frechen, 2006; Molliex et al., 2013). In Corsica, the same process can be evoked, because post-
557 Miocene exhumation and Quaternary glaciations of the inner part of Corsica (Fellin et al., 2005a) is concomitant
558 with a higher frequency in Hercynian clasts in alluvial deposits. The change in pebbles composition at the 40 m
559 depth in the borehole supports the hypothesis that the sediments located above this depth started to be accumulated
560 after the Mid-Pleistocene transition.

561 In summary, the upper 40 m-depth of the borehole GBEC5-2 were likely deposited after the Mid-Pleistocene
562 transition, during the Late Pleistocene and the Holocene, with an accumulation rate of about 40-50 m Ma⁻¹. They

563 are mainly composed of material from the higher Hercynian part of the Corsican reliefs. This observation is
564 consistent with an enhancement of the erosional flux from high elevation areas under the glacial conditions of the
565 Late Pleistocene (100 ka glacial cycles), as also documented in the French Alps (Dubar, 1984; Colomb et Roux,
566 1978). The deposits below ~60 m-depth are constituted by a higher part of Alpine content and could thus be related
567 to pre-glacial conditions, such as those of the Early Pleistocene. There is no evidence of marine sedimentation
568 between 2.6 and 0.9 Ma, thus Early Pleistocene deposits of the Golo River plain reflect continental conditions for
569 a long time, between their deposition (2-3 Ma) and the onset of the Mid-Pleistocene transition (0.9 Ma; Gibbard
570 et al., 2010). The sediment included between ~40 and 60 m-depth could thus be interpreted as the weathered zone
571 of Early Pleistocene deposits. A tilting of the margin with low subsidence rates in the plain (~ 0.03 mm yr⁻¹) should
572 have occurred at least during the Early Pleistocene and perhaps more recently. It is probably superimposed with
573 the motion of a normal fault located in the upstream alluvial plain. Confirming the existence of this fault could
574 motivate future research.

575

576 6- CONCLUSION

577 For a better understanding of the Quaternary evolution of the Golo River alluvial plain, we obtained data from
578 several approaches, including geomorphology, soil studies, sedimentology, ERT profile and terrestrial cosmogenic
579 nuclides dating (¹⁰Be and ²⁶Al). We improved the accuracy and resolution of geological mapping of Quaternary
580 alluvial sheets in the Golo plain and provided new chronological constrains based on soil chronosequence and
581 cosmogenic nuclides. We highlighted at least four alluvial terraces within the Golo coastal plain. Their deposition
582 are related to sea-level variations and occurred during sea-level highstands, while incision of the plain occurred
583 during sea-level lowstands. Based on a new ¹⁰Be depth-profile, the abandonment age of terrace Fy2 is at least 70
584 ka, older than it was previously suggested by luminescence dating (~50 ka). This discrepancy between existing
585 luminescence ages and cosmogenic nuclide-based chronology might be due to a difference in the type (grain size)
586 of analyzed sediment. Finer sandy fraction could reflect a soil bioturbation event (dated at ~50 ka by IRSL) that
587 occurred several thousand years after the terrace deposition (dated before 70 ka by ¹⁰Be). More detailed studies
588 are required to check this point. Furthermore, we recognized in the GBEC5-2 borehole a thick amount of alluvial
589 deposits (> 117 m), including an unknown formation which lies below the Quaternary alluvial sheets outcropping
590 in the plain. This continental formation, dated at 2.5-3 Ma by the ²⁶Al/¹⁰Be burial chronometer, can be interpreted
591 as an infill of an Early Pleistocene accommodation space caused by the subsidence of the area at a rate ~ 0.03 mm
592 yr⁻¹. An unidentified fault is probably delimiting the eastern subsidence plain and the western highlands. Because
593 of its large thickness and despite its moderate lateral extent, the Golo alluvial plain has to be considered as a
594 potential significant storage area in source-to-sink studies.

595

596 ACKNOWLEDGEMENTS

597 This research was financed by IFREMER, the "Agence de l'Eau Rhône-Méditerranée-Corse" and also benefited
598 from a State Grant from the French "Agence Nationale de la Recherche (ANR)" in the Program "Investissements
599 d'Avenir" (ANR-10-LABX-19-01, Labex Mer). It was finalized as part of the EROMED ANR program (ANR-17-
600 CE01-0011). JEAS was funded by ALW-NWO (Dutch Organization for Scientific Research, VIDI grant number
601 864.09.004). We warmly thank Daniel Hermitte, Jean-Claude Parisot, Phillipe Dussouillez for their assistance with
602 ERT and GPS on field, and Angélique Roubi and Nicolas Freslon who were involved in the field explorations and

603 drilling operation. We also thank Francois Galgani and Gwenaëlle Bodéré, respectively from IFREMER and
604 BRGM centers in Corsica; for the on-site logistical support. CICO quarry, Jean-Louis Cipriani, the Lucchiana city
605 and the “Mariana et la basse vallée du Golo” association are thanked for their local assistance on field. Elodie Petit
606 and Ewan Pelleter are thanked for their help in petrography. ^{10}Be measurements at the ASTER AMS national
607 facility (CEREGE, Aix en Provence) is supported by the INSU/CNRS, the ANR through the "Projets thématiques
608 d'excellence" program for the "Equipements d'excellence" ASTER-CEREGE action, and IRD. The French CNRS
609 INSU SYSTER partly financed cosmogenic nuclide concentration measurements. ^{10}Be and ^{26}Al measurement at
610 the PRIME AMS facility was performed by MW Caffee and his team. We also warmly thank N. Akçar, T.
611 Reimann, an anonymous reviewer and editor F. Preusser for their fruitful comments that considerably improved
612 the first version of the manuscript.

613

614 REFERENCES

615

- 616 Allen, P.A., 2008. Time scales of tectonic landscapes and their sediment routing systems, in Gallagher, K., Jones,
617 S. J., and Wainwright, J., ed., *Landscape Evolution: Denudation, Climate and Tectonics over Different*
618 *Time and Space Scales*. Geological Society of London, Special Publication 276, 7-28.
- 619 Arnold, M., Merchel, S., Bourles, D.L., Braucher, R., Benedetti, L., Finkel, R.C., Aumaitre, G., Gottang, A.,
620 Klein, M., 2010. The French accelerator mass spectrometry facility ASTER: Improved performance and
621 developments: Nuclear Instruments & Methods in Physics Research Section B-Beam Interactions with
622 Materials and Atoms 268, 1954-1959.
- 623 Auclair, M., Lamothe, M., Huot, S., 2003. Measurement of anomalous fading for feldspar IRSL using SAR.
624 Radiation measurements 37(4-5), 487-492.
- 625 Auclair, M., Lamothe, M., Lacroix, F., Banerjee, S.K., 2007. Luminescence investigation of loess and tephra from
626 Halfway House section, Central Alaska. Quaternary Geochronology 2(1-4), 34-38.
- 627 Baize, D., Girard, M.C., 2008. *Référentiel Pédologique : classification des sols établie en France*. Editions Quae,
628 403 pp.
- 629 Balco, G., Stone, J.O., Lifton, N.A., Dunai, T.J., 2008. A complete and easily accessible means of calculating
630 surface exposure ages or erosion rates from ^{10}Be and ^{26}Al measurements. Quat. Geochronol. 3, 174–195.
- 631 Blard, P.H., Lupker, M., Rousseau, M., 2019a. Paired-cosmogenic nuclide paleoaltimetry. Earth and Planetary
632 Science Letters 515, 271-282.
- 633 Blard, P.H., Lupker, M., Rousseau, M., Tesson, J., 2019b. Two MATLAB programs for computing paleo-elevations
634 and burial ages from paired-cosmogenic nuclides. MethodsX 6, 1547-1556
635 (<https://doi.org/10.1016/j.mex.2019.05.01>).
- 636 Blum, M.D., Törnqvist, T.E., 2000. Fluvial responses to climate and sea-level change: A review and look forward.
637 Sedimentology 47, 2–48.
- 638 Blum, M., Martin, J., Milliken, K., Garvin, M., 2013. Paleovalley systems: Insights from Quaternary analogs and
639 experiments. Earth-Science Rev. 116, 128–169.
- 640 Boenigk, W., Frechen, M. 2006. The Pliocene and Quaternary fluvial archives of the Rhine system. Quaternary
641 Science Reviews 25(5-6), 550-574.

642 Bornand, M., 1978. Altération des matériaux fluvio-glaciaires, genèse et évolution des sols sur terrasses
643 quaternaires dans la moyenne vallée du Rhône. State Thesis, Université du Languedoc. 329 pp.

644 Braucher, R., Del Castillo, P., Siame, L., Hidy, A.J., Bourles, D.L., 2009. Determination of both exposure time
645 and denudation rate from an in situ-produced Be-10 depth profile: A mathematical proof of uniqueness.
646 Model sensitivity and applications to natural cases. *Quaternary Geochronology* 4, 56-67.

647 Braucher, R., Merchel, S., Borgomano, J., Bourles, D.L., 2011. Production of cosmogenic radionuclides at great
648 depth: A multi element approach. *Earth and Planetary Science Letters* 309, 1-9.

649 Brocard, G. Y., van der Beek, P. A., Bourlès, D. L., Siame, L.L., Mugnier, J.-L., 2003. Long-term fluvial incision
650 rates and postglacial river relaxation time in the French Western Alps from ¹⁰Be dating of alluvial terraces
651 with assessment of inheritance, soil development and wind ablation effects. *Earth and Planetary Science*
652 *Letters* 209, 197-214.

653 Buylaert, J. P., Vandenberghe, D., Murray, A. S., Huot, S., De Corte, F., Van den Haute, P., 2007. Luminescence
654 dating of old (> 70 ka) Chinese loess: a comparison of single-aliquot OSL and IRSL techniques. *Quaternary*
655 *Geochronology* 2(1-4), 9-14.

656 Buylaert, J. P., Jain, M., Murray, A. S., Thomsen, K. J., Thiel, C., Sohbaty, R., 2012. A robust feldspar
657 luminescence dating method for Middle and Late Pleistocene sediments. *Boreas* 41(3), 435-451.

658 Calves, G., Toucanne, S., Jouet, G., Charrier, S., Thereau, E., Etoubleau, J., Marsset, T., Droz, L., Bez, M., Abreu,
659 V., Jorry, S., Mulder, T., Lericolais, G., 2013. Inferring denudation variations from the sediment record; an
660 example of the last glacial cycle record of the Golo Basin and watershed, East Corsica, western
661 Mediterranean sea. *Basin Research* 25, 197-218.

662 Carr, A.S., Hay, A.S., Powell, D.M., Livingstone, I., 2019. Testing post-IR IRSL luminescence dating methods in
663 the southwest Mojave Desert, California, USA. *Quaternary Geochronology* 49, 85-91.

664 Champagnac, J.D., Molnar, P., Anderson, R.S., Sue, C., Delacou, B., 2007. Quaternary erosion-induced isostatic
665 rebound in the western Alps. *Geology* 35(3), 195-198.

666 Chantraine, J., Autran, A., Cavelier, C., 1996. Geological map of France (1/1 000 000). Ed. BRGM: Orléans.

667 Colomb, E., Roux, R.-M., 1978. La Crau. Données nouvelles et interprétations. *Géologie méditerranéenne*, V(3),
668 303-324.

669 Conchon, O., 1975. Les formations quaternaires de type continental en Corse orientale. PhD thesis, Univ. Paris 6.

670 Conchon, O., 1977. Néotectonique en Corse orientale d'après l'étude des formations quaternaires : comparaison
671 entre la Marana et la plaine d'Aléria. *Bulletin de la Société Géologique de France* 7, 631-639.

672 Conchon, O., 1978. Quaternary Studies in Corsica (France). *Quaternary Research* 9, 41-53.

673 Conchon, O., 1980, Stratigraphie du Quaternaire en Corse, in Chaline, J., ed., *Problèmes de stratigraphie*
674 *quaternaire en France et dans les pays limitrophes*, AFEQ editions, 332-342.

675 Conchon, O., 1986. Quaternary Glaciations in Corsica. *Quaternary Science Reviews* 5, 429-432.

676 Conchon, O., 1989. Dynamique et chronologie du détritisme quaternaire en Corse, domaine méditerranéen
677 montagnard et littoral. *Bull. Asso. Fr. Et. Quat.* 26(4), 201-211.

678 Conchon, O., 1999. Le littoral Corse au Quaternaire. *Quaternaire* 10, 95-105.

679 Crook, N., Binley, A., Knight, R., Robinson, D.A., Zarnetske, J., Haggerty, R., 2008. Electrical resistivity imaging
680 of the architecture of substream sediments. *Water Resources Research* 44, W00D13,
681 doi:10.1029/2008WR006968.

682 Danisik, M., Kuhlemann, J., Dunkl, I., Szekely, B., Frisch, W., 2007. Burial and exhumation of Corsica (France)
683 in the light of fission track data. *Tectonics* 26, TC1001, doi:10.1029/2005TC001938.

684 de Boer, B., Van de Wal, R.S.W., Bintanja, R., Lourens, L.J., Tuenter, E., 2010. Cenozoic global ice-volume and
685 temperature simulations with 1-D ice-sheet models forced by benthic $\delta^{18}O$ records. *Ann. Glaciol.* 51, 23–
686 33.

687 Delmas, M., Braucher, R., Gunnell, Y., Guillou, V., Calvet, M., Bourlès, D., 2015. Constraints on Pleistocene
688 glaciofluvial terrace age and related soil chronosequence features from vertical ^{10}Be profiles in the Ariège
689 River catchment (Pyrenees, France). *Glob. Planet. Change* 132, 39–53.

690 Delmas, M., Calvet, M., Gunnell, Y., Voinchet, P., Manel, C., Braucher, R., Tissoux, H., Bahain, J.J., Perrenoud,
691 C., Saos, T., 2018. Terrestrial ^{10}Be and electron spin resonance dating of fluvial terraces quantifies
692 quaternary tectonic uplift gradients in the eastern Pyrenees. *Quat. Sci. Rev.* 193, 188–211.

693 Demartini, J., Favreau, P., 2011. *Référentiel Pédologique Approfondi (RPA). Caractérisation des sols de plaines*
694 *et coteaux de basse altitude au 1:25.000, ODARC.*

695 Dubar, M., 1984. Chronologie et signification des dépôts continentaux du Néogène supérieur du bassin de Riez-
696 Valensole (Alpes-de-Haute-Provence, France). *Bull. Soc. Géol. Fr (7) XXVI*, 5, 971-978.

697 Duller, G.A.T., 1994. Luminescence dating using feldspars: a test case from southern North Island, New Zealand.
698 *Quaternary Science Reviews* 13(5-7), 423-427.

699 Dunai, T.J., 2010. *Cosmogenic Nuclides: Principles, Concepts and Applications in Earth Surface Sciences: New*
700 *York, Cambridge University Press, 187 pp.*

701 Durand, N., Gunnell, Y., Curmi, P., Ahmad, M., 2007. Pedogenic carbonates on Precambrian metamorphic rocks
702 in South India: origin and paleoclimatic significance. *Quat. Int.* 162–163, 35–49.

703 Fan, Y.X., Zhao, H., Chen, F.H., 2010. The equivalent dose of different grain size quartz fractions from lakeshore
704 sediments in the arid region of north China. *Quaternary Geochronology* 5(2-3), 205-211.

705 FAO, 2014. *World reference base for soil resources. International soil classification system for naming soils and*
706 *creating legends for soil maps. World soil resources report 106, 192 pp.*

707 Fellin, M.G., Picotti, V., Zattin, M., 2005a. Neogene to Quaternary rifting and inversion in Corsica: Retreat and
708 collision in the western Mediterranean. *Tectonics* 24, TC1011, doi:10.1029/2003TC001613.

709 Fellin, M.G., Zattin, M., Picotti, V., Reiners, P.W., Nicolescu, S., 2005b. Relief evolution in northern Corsica
710 (western Mediterranean): Constraints on uplift and erosion on long-term and short-term timescales. *Journal*
711 *of Geophysical Research-Earth Surface* 110, F01016, doi:10.1029/2004JF000167.

712 Fellin, M.G., Vance, J.A., Garver, J.I., Zattin, M., 2006. The thermal evolution of Corsica as recorded by zircon
713 fission-tracks. *Tectonophysics* 421, 299-317.

714 Forzoni, A., Storms, J. E. A., Reimann, T., Moreau, J., Jouet, G., 2015. Non-linear response of the Golo River
715 system, Corsica, France, to Late Quaternary climatic and sea level variations. *Quaternary Science Reviews*
716 121, 11-27.

717 Fournier, M., Jolivet, L., Goffe, B., Dubois, R., 1991. Alpine Corsica Metamorphic Core Complex. *Tectonics* 10,
718 1173-1186.

719 Gibbard, P. L., Head, M. J., Walker, M. J. C. and the Subcommission on Quaternary Stratigraphy. 2010. Formal
720 ratification of the Quaternary System/Period and the Pleistocene Series/Epoch with a base at 2.58 Ma. *J.*
721 *Quaternary Sci.* 25, 96–102.

- 722 Gosse, J.C., Phillips, F.M., 2001. Terrestrial in situ cosmogenic nuclides: theory and application. *Quaternary*
723 *Science Reviews* 20, 1475-1560.
- 724 Gourry, J.C., Vermeersch, F., Garcin, M., Giot, D., 2003. Contribution of geophysics to the study of alluvial
725 deposits: a case study in the Val d'Avaray area of the River Loire, France. *Journal of Applied Geophysics*
726 54, 35-49.
- 727 Granger, D.E., Kirchner, J.W., Finkel, R., 1996. Spatially averaged long-term erosion rates measured from in situ-
728 produced cosmogenic nuclides in alluvial sediment. *The Journal of Geology* 104(3), 249-257.
- 729 Hancock, G.S., Anderson, R.S., Chadwick, O.A., Finkel, R.C., 1999. Dating fluvial terraces with ^{10}Be and ^{26}Al
730 profiles: Application to the Wind River, Wyoming. *Geomorphology* 27(1-2), 41-60.
- 731 Harris, L., 1985, Progressive and Polyphase Deformation of the Schistes Lustres in Cap Corse, Alpine Corsica.
732 *Journal of Structural Geology* 7, 637-650.
- 733 Herman, F., Seward, D., Valla, P.G., Carter, A., Kohn, B., Willett, S.D., Ehlers, T.A., 2013. Worldwide
734 acceleration of mountain erosion under a cooling climate. *Nature* 504(7480), 423.
- 735 Hidy, A.J., Gosse, J.C., Pederson, J.L., Mattern, J.P., Finkel, R.C., 2010. A geologically constrained Monte Carlo
736 approach to modeling exposure ages from profiles of cosmogenic nuclides: An example from Lees Ferry,
737 Arizona. *Geochemistry Geophysics Geosystems* 11, Q0AA10, doi:10.1029/2010GC003084.
- 738 Hubschman, J., 1973. Etablissement par l'étude des faciès d'altération, d'un schéma stratigraphique du Quaternaire
739 garonnais et ariégeois. *C. R. Acad. Sci. D* 277, 753-755.
- 740 Hughes, P.D., Gibbard, P.L., 2018. Global glacier dynamics during 100 ka Pleistocene glacial cycles. *Quaternary*
741 *Research* 2018, 1-22.
- 742 Jeong, G.Y., Cheong, C.S., Choi, J.H., 2007. The effect of weathering on optically stimulated luminescence dating.
743 *Quaternary Geochronology* 2(1-4), 117-122.
- 744 Kars, R.H., Wallinga, J., Cohen, K.M., 2008. A new approach towards anomalous fading correction for feldspar
745 IRSL dating—tests on samples in field saturation. *Radiation Measurements* 43(2-6), 786-790.
- 746 Kars, R.H., Busschers, F.S., Wallinga, J., 2012. Validating post IR-IRSL dating on K-feldspars through
747 comparison with quartz OSL ages. *Quaternary Geochronology* 12, 74-86.
- 748 Krumrei, I., 2009, Würmian glaciation and climate in the western Mediterranean based on investigations in the
749 mountain chain of Corsica. PhD thesis, Tübingen, Eberhard-Karls-Universität.
- 750 Kuhlemann, J., Frisch, W., Szekely, B., Dunki, I., Danisik, M., Krumrei, I., 2005. Würmian maximum glaciation
751 in Corsica: glacier extent, amplifying paleorelief, and mesoscale climate. *Austrian Journal of Earth Sciences*
752 97, 68-81.
- 753 Kuhlemann, J., Rohling, E.J., Krumrei, I., Kubik, P., Ivy-Ochs, S., Kucera, M., 2008a, Regional synthesis of
754 Mediterranean atmospheric circulation during the last glacial maximum. *Science* 321, 1338-1340.
- 755 Kuhlemann, J., van der Borg, K., Bons, P.D., Danisik, M., Frisch, W., 2008b. Erosion rates on subalpine
756 paleosurfaces in the western Mediterranean by in-situ Be-10 concentrations in granites: implications for
757 surface processes and long-term landscape evolution in Corsica (France): *International Journal of Earth*
758 *Sciences* 97, 549-564.
- 759 Lahondère, J.-C., Conchon, O., Lahondère, D., 1994. Vescovato, Carte Géologique de la France, BRGM, Feuille
760 1107, échelle 1:50.000: Orléans, France.

- 761 Le Dortz, K., Meyer, B., Sebrier, M., Braucher, R., Bourles, D., Benedetti, L., Nazari, H., Foroutan, M., 2012.
762 Interpreting scattered in-situ produced cosmogenic nuclide depth-profile data: Quaternary Geochronology
763 11, 98-115.
- 764 Legros, J. P., 2012. Major Soil Groups of the World: Ecology, Genesis, Properties and Classification. CRC Press,
765 447 pp.
- 766 Li, B., Li, S.H., 2011. Luminescence dating of K-feldspar from sediments: a protocol without anomalous fading
767 correction. Quaternary Geochronology 6(5), 468-479.
- 768 Li, Y., Tsukamoto, S., Frechen, M., Gabriel, G., 2018. Timing of fluvial sedimentation in the Upper Rhine Graben
769 since the Middle Pleistocene: constraints from quartz and feldspar luminescence dating. Boreas 47(1), 256-
770 270.
- 771 Loke, M.H., Barker, R.D., 1996. Rapid least-squares inversion of apparent resistivity pseudosections by a quasi-
772 Newton method, Geophysical Prospecting 44, 131-152.
- 773 Lowick, S.E., Preusser, F., 2011. Investigating age underestimation in the high dose region of optically stimulated
774 luminescence using fine grain quartz. Quaternary Geochronology 6(1), 33-41.
- 775 Lowick, S.E., Valla, P.G., 2018. Characterising the luminescence behaviour of ‘infinitely old’ quartz samples from
776 Switzerland. Quaternary geochronology 43, 1-11.
- 777 Loÿe-Pilot, M.D., Durand-Delga, M., Feinberg, H., Gourinard, Y., Magne, J., 2004. The Burdigalian of eastern
778 Corsica within its geodynamic setting. Comptes Rendus Geoscience 336, 919-930.
- 779 Martin, L.C.P., Blard, P.H., Balco, G., Lavé, J., Delunel, R., Lifton, N., Laurent, V., 2017. The CREp program
780 and the ICE-D production rate calibration database: A fully parameterizable and updated online tool to
781 compute cosmic-ray exposure ages. Quat. Geochronol. 38, 25–49.
782 <https://doi.org/10.1016/j.quageo.2016.11.006>
- 783 Mattauer, M., Faure, M., Malavieille, J., 1981. Transverse Lineation and Large-Scale Structures Related to Alpine
784 Obduction in Corsica. Journal of Structural Geology 3, 401-409.
- 785 Merchel, S., Arnold, M., Aumaitre, G., Benedetti, L., Bourlès, D.L., Braucher, R., Alfimov, V., Freeman, S.P.H.T.,
786 Steier, P., Wallner, A., 2008. Towards more precise ¹⁰Be and ³⁶Cl data from measurements at the 10-14
787 level: Influence of sample preparation. Nuclear Instruments and Methods in Physics Research B 266, 4921-
788 4926.
- 789 Miller, K.G., Kominz, M.A., Browning, J.V., Wright, J.D., Mountain, G.S., Katz, M.E., Sugarman, P.J., Cramer,
790 B.S., Christie-Blick, N., Pekar, S.F., 2005. The Phanerozoic record of global sea-level change. Science 310,
791 1293–1298.
- 792 Milner, A.M., Collier, R.E.L., Roucoux, K.H., Müller, U.C., Pross, J., Kalaitzidis, S., Christanis, K., Tzedakis,
793 P.C., 2012. Enhanced seasonality of precipitation in the Mediterranean during the early part of the Last
794 Interglacial. Geology 40, 919–922.
- 795 Mix, A.C., Bard, E., Schneider, R., 2001. Environmental processes of the ice age: land, oceans, glaciers (EPILOG).
796 Quaternary Science Reviews, 20(4) 627-657.
- 797 Molliex, S., 2009. Caractérisation de la déformation tectonique récente en Provence (SE France). PhD thesis, Univ.
798 Aix-Marseille III, 350 pp.

799 Molliex, S., Siame, L., Bourlès, D.L., Braucher, R., Bellier, O., Clauzon, G., 2013. Quaternary evolution of a large
800 alluvial fan in a peri-glacial setting (Crau plain, SE France), constrained by terrestrial cosmogenic nuclide
801 (^{10}Be). *Geomorphology* 195, 45–52.

802 Molliex, S., Jouet, J., Freslon, N., Bourlès, D.L., Authemayou, C., Moreau, J., Rabineau, M., 2017. Controls on
803 Holocene denudation rates in mountainous environments under Mediterranean climate. *Earth Surface
804 Processes and Landforms* 42(2), 272-289. doi: 10.1002/esp.3987

805 Muscheler, R., Beer, J., Kubik, P.W., Synal, H.A., 2005. Geomagnetic field intensity during the last 60,000 years
806 based on ^{10}Be and ^{36}Cl from the Summit ice cores and ^{14}C . *Quat. Sci. Rev.* 24, 1849–1860.
807 <https://doi.org/10.1016/j.quascirev.2005.01.012>

808 Nishiizumi, K., 2004. Preparation of ^{26}Al AMS standards. *Nuclear Instruments and Methods in Physics Research
809 Section B: Beam Interactions with Materials and Atoms* 223, 388-392.

810 Nishiizumi, K., Imamura, M., Caffee, M. W., Southon, J. R., Finkel, R. C., McAninch, J., 2007. Absolute
811 calibration of ^{10}Be AMS standards. *Nuclear Instruments and Methods in Physics Research Section B:
812 Beam Interactions with Materials and Atoms* 258(2), 403-413.

813

814 Pedoja, K., Husson, L., Regard, V., Cobbold, P.R., Ostanciaux, E., Johnson, M.E., Kershaw S., Saillard, M.,
815 Martinod, J. Furgerot, L., Weill, P., Delcaillau, B., 2011. Relative sea-level fall since the last interglacial
816 stage: are coasts uplifting worldwide? *Earth-Science Reviews* 108(1-2), 1-15.

817 Pedro, G., 1968. Distribution des principaux types d'altération chimique à la surface du globe. Présentation d'une
818 esquisse géographique: *Revue de Géographie Physique et Géologie Dynamique* 10, 457-470.

819 Petit, C., Campy, M., Chaline, J., Bonvalot, J., 1996. Major palaeohydrographic changes in Alpine foreland during
820 the Pliocene-Pleistocene. *Boreas* 25(2), 131-143.

821 Peyron, O., Guiot, J., Cheddadi, R., Tarasov, P., Reille, M., de Beaulieu, J.L., Bottema, S., Andrieu, V., 1998.
822 Climatic reconstruction in Europe for 18,000 yr B.P. from pollen data. *Quaternary Research* 49, 183-196.

823 Reille, M., Gamisans, J., deBeaulieu, J.L., Andrieu, V., 1997. The late-glacial at Lac de Creno (Corsica, France):
824 A key site in the western Mediterranean Basin. *New Phytologist* 135, 547-559.

825 Reille, M., Gamisans, J., Andrieu-Ponel, V., De Beaulieu, J.-L., 1999. The Holocene at Lac de Creno, Corsica,
826 France : a key site for the whole island. *New Phytologist* 141, 291–307.

827 Reimann, T., Román-Sánchez, A., Vanwalleghem, T., & Wallinga, J., 2017. Getting a grip on soil reworking–
828 Single-grain feldspar luminescence as a novel tool to quantify soil reworking rates. *Quaternary
829 Geochronology* 42, 1-14.

830 Rohling, E.J., 1994. Review and new aspects concerning the formation of eastern Mediterranean sapropels. *Mar.
831 Geol.* 122, 1–28.

832 Rohling, E.J., Foster, G.L., Grant, K.M., Marino, G., Roberts, A.P., Tamsiea, M.E., Williams, F., 2014. Sea-level
833 and deep-sea-temperature variability over the past 5.3 million years. *Nature* 508(7497), 477–482.

834 Rohling, E.J., Marino, G., Grant, K.M., 2015. Mediterranean climate and oceanography, and the periodic
835 development of anoxic events (sapropels). *Earth-Science Rev.* 143, 62–97.

836 Saint-Carlier, D., Charreau, J., Lavé, J., Blard, P.H., Dominguez, S., Avouac, J.P., Wang, S., Arnold, M., Aumaître,
837 G., Keddadouche, K., Léanni, L., Chauvet, F., Bourlés, D.L., 2016. Major temporal variations in shortening

838 rate absorbed along a large active fold of the southeastern Tianshan piedmont (China). *Earth Planet. Sci.*
839 *Lett.* 434, 333–348.

840 Sasaki, Y., 1992. Resolution of resistivity tomography inferred from numerical simulation. *Geophysical*
841 *Prospecting* 40, 453-464.

842 Serrano, O., Allanic, C., Magar, M., 2013. Synthèse géologique du bassin tertiaire de la plaine orientale corse.
843 Liaison terre-mer entre Nicolao et Solenzara. BRGM report RP62303FR. 181 pp.

844 Siame, L., Bellier, O., Braucher, R., Sebrier, M., Cushing, M., Bourles, D., Hamelin, B., Baroux, E., de Voogd,
845 B., Raisbeck, G., Yiou, F., 2004. Local erosion rates versus active tectonics: cosmic ray exposure modelling
846 in Provence (south-east France). *Earth and Planetary Science Letters* 220, 345-364.

847 Skyles, E.M., 2013. Alluvial geochronology and watershed analysis of the Golo River, Northeastern Corsica,
848 France. Msc thesis, Logan, Utah State University.

849 Sømme, T.O., Piper, D.J.W., Deptuck, M.E., Helland-Hansen, W., 2011. Linking Onshore-Offshore Sediment
850 Dispersal in the Golo Source-to-Sink System (Corsica, France) during the Late Quaternary. *Journal of*
851 *Sedimentary Research* 81, 118-137.

852 Spratt, R.M., Lisiecki, L.E., 2016. A Late Pleistocene sea level stack. *Clim. Past* 12, 1079–1092.

853 Steffen, D., Preusser, F., Schlunegger, F., 2009. OSL quartz age underestimation due to unstable signal
854 components. *Quaternary Geochronology* 4(5), 353-362.

855 Stone, J.O., 2000. Air pressure and cosmogenic isotope production. *Journal of Geophysical Research-Solid Earth*
856 105, 23753-23759.

857 Sweet, M.L., Gaillot, G.T., Jouet, G., Rittenour, T.M., Toucanne, S., Marsset, T., Blum, M.D., 2020. Sediment
858 routing from shelf to basin floor in the Quaternary Golo System of Eastern Corsica, France, western
859 Mediterranean Sea. *Geological Society of America Bulletin* 132 (5-6): 1217–1234.

860 Thiel, C., Buylaert, J. P., Murray, A., Terhorst, B., Hofer, I., Tsukamoto, S., Frechen, M., 2011. Luminescence
861 dating of the Stratzing loess profile (Austria)–Testing the potential of an elevated temperature post-IR IRSL
862 protocol. *Quaternary International* 234(1-2), 23-31

863 Timar, A., Vandenbergh, D., Panaiotu, E. C., Panaiotu, C. G., Necula, C., Cosma, C., 2010. Optical dating of
864 Romanian loess using fine-grained quartz. *Quaternary Geochronology*, 5(2-3) 143-148.

865 Timar-Gabor, A., Buylaert, J.P., Guralnik, B., Trandafir-Antohei, O., Constantin, D., Anechitei-Deacu, V., Jain,
866 M., Murray, A.S, Porat, N., Hao, Q., Wintle, A.G., 2017. On the importance of grain size in luminescence
867 dating using quartz. *Radiation Measurements* 106, 464-471.

868 Toucanne, S., Minto'o, C. M. A., Fontanier, C., Bassetti, M. A., Jorry, S. J., Jouet, G., 2015. Tracking rainfall in
869 the northern Mediterranean borderlands during sapropel deposition. *Quaternary Science Reviews* 129, 178-
870 195.

871 Twidale, CR., 2004. River patterns and their meaning. *Earth-Science Reviews* 67(3-4), 159-218.

872 Uppala, S.M., Kållberg, P.W., Simmons, A.J., Andrae, U., da Costa Bechtold, V., Fiorino, M., Gibson, J.K.,
873 Haseler, J., Hernandez, A., Kelly, G.A., Li, X., Onogi, K., Saarinen, S., Sokka, N., Allan, R.P., Andersson,
874 E., Arpe, K., Balmaseda, M.A., Beljaars, A.C.M., van de Berg, L., Bidlot, J., Bormann, N., Caires, S.,
875 Chevallier, F., Dethof, A., Dragosavac, M., Fisher, M., Fuentes, M., Hagemann, S., Hólm, E., Hoskins,
876 B.J., Isaksen, L., Janssen, P.A.E.M., Jenne, R., McNally, A.P., Mahfouf, J.F., Morcrette, J.J., Rayner, N.A.,

877 Saunders, R.W., Simon, P., Sterl, A., Trenberth, K.E., Untch, A., Vasiljevic, D., Viterbo, P., Woollen, J.,
878 2005. The ERA-40 re-analysis. *Q. J. R. Meteorol. Soc.* 131, 2961–3012. <https://doi.org/10.1256/qj.04.176>
879 Valla, PG., Shuster, DL., Van Der Beek, PA., 2011. Significant increase in relief of the European Alps during
880 mid-Pleistocene glaciations. *Nature geoscience* 4(10), 688.
881 Vreken, W.J., 1975. Principal kinds of chronosequences and their significance in soil history. *J. Soil Sci.* 26,
882 378–394.
883 Wintle, A.G. 1973. Anomalous fading of thermo-luminescence in mineral samples. *Nature* 245(5421), 143-144.
884
885

886 FIGURE CAPTIONS

- 887 1) Geomorphological and geological setting of the Golo River catchment (modified from Molliex et al.,
888 2017). A) Topographic map. B) Geological map (from Chantraine et al., 1996). LGM glaciers extent from
889 Kuhlemann et al., (2005).
890
- 891 2) Morphologic map of the Golo alluvial plain. Morphological areas are defined on the basis of slope breaks.
892 Locations of topographic and soil-related profiles of Fig.3.
893
- 894 3) Topographic profiles of the Golo alluvial plain (location in Fig. 2), with soil related correspondence. A)
895 A-B-C-D profiles are West-East oriented (longitudinally to Golo present-day Valley); B) E-F-G profiles
896 are South-North oriented (transversally to the Golo present-day Valley). C) Relationship between
897 elevation and slope of each pixel of the plain according to the type of soil and the definition of
898 morphologic areas (Upper, Middle and Lower plain). In the three sub-figures, morphological areas are
899 represented by the grey-scale background.
900
- 901 4) Classification of alluvial soils of the Golo alluvial plain. A) Synthetic typical logs from the different
902 terraces of the Golo alluvial plain. B) Pictures illustrating the typical types of soils from the Golo alluvial
903 plain terraces. C) Relative abundance of soil evolution weathering processes for each terrace. Modified
904 from Demartini and Favreau (2011).
905
- 906 5) Updated geological map of Quaternary formations of the Golo coastal plain, based on morphology,
907 sedimentology and soil characteristics. The black dashed line shows the extent of Golo deposits. Insert in
908 top right corner represent the location of soil data from Demartini and Favreau (2011).
909
- 910 6) Gol10 (A) and Gol06 (B) Electrical Resistivity Image (ERI) and interpretations obtained with a
911 Schlumberger protocol, 64 electrodes, 10m-spacing, 630 m- and 950 m-long, respectively, with a 90m-
912 deep penetration. Interpretations are based on surface geology, borehole data and contrasts of resistivity.
913 Location of profiles is indicated in Fig. 5.
914
- 915 7) A) GBEC5-2 lithologic and stratigraphic log. (X = 9.45532°E; Y = 42.52767°N; Z = 18 m, location on
916 Fig. 5) B) Statistics on pebbles content along the GBEC5-2 borehole. C) Some representative pictures of
917 each formation, with true color and scale.

- 918
- 919 8) Cosmogenic ^{10}Be dating of the Fy2 terrace at the CICO gravel pit (location on Fig. 5). A - Picture of the
- 920 Fy2 CICO gravel pit outcrop showing the samples analyzed for in situ cosmogenic ^{10}Be . B - Measured
- 921 cosmogenic ^{10}Be concentration in quartz (at.g^{-1}) vs sampling depth. Red curve is the modeled best-fit
- 922 attenuation profile, including production by spallation and muons. Used parameters are: a world average
- 923 SLHL production rate of $4.13 \pm 0.20 \text{ at.g}^{-1} \cdot \text{yr}^{-1}$ (CREp calculator; Martin et al., 2017), with the Lal/Stone
- 924 time dependent scaling (Stone, 2000; Balco et al., 2008), the ERA40 atmosphere (Uppala et al., 2005)
- 925 and the geomagnetic reconstruction of Muscheler et al., 2005. Muonic production is modeled with the
- 926 exponential attenuation profile and the parameters defined in (Braucher et al., 2011). C - Most probable
- 927 exposure erosion solutions represented as Khi-2 values for variable erosion and exposure time couples.
- 928 These estimates are obtained using the Monte Carlo best-fit modeling approach of Saint-Carlier et al.
- 929 (2016). This algorithm is a development of the (Hidy et al., 2010) model that takes into account the
- 930 stochastic variability and the uncertainty of the inherited component. Our inversion shows that the ^{10}Be
- 931 profile requires a minimum exposure duration of 70 ka and a maximum denudation rate of $10 \pm 2 \text{ mm.ka}^{-1}$.
- 932 D - Estimate of the inherited ^{10}Be component.
- 933
- 934 9) Photos of luminescence IRSL sample sites. A1) CICO Fy2 terrace site. A2) Zoom on the CICO sample
- 935 zone. The black arrows show bioturbations in sediment caused by rooted vegetation. B1) SINI Fy1 terrace
- 936 site. B2) Zoom on the SINI sample zone. White squares on A1 and B1 correspond to the extent of photo
- 937 A2 and B2 respectively. CICO and SINI samples position can be found in Fig. 5 and Table 4.
- 938
- 939 10) Interpretation of GBEC5-2 borehole in its geological setting. A) Outcrop of the base of the highest
- 940 Quaternary terrace (Fy1) just upstream of the alluvial plain (location in B). B) Local geological map of
- 941 GBEC5-2 setting. C) Longitudinal profile of Golo River and geological interpretative cross-section. D)
- 942 Picture of the base of GBEC5 borehole, showing alluvial braided material at 117.4 m below ground floor.
- 943
- 944

945 TABLE CAPTIONS

- 946 1) Characteristics of Golo alluvial terraces with a comparison of estimated published ages
- 947
- 948 2) ^{10}Be data along the depth profile of CICO gravel pit ($X = 9.4878^\circ\text{E}$; $Y = 42.5495^\circ\text{N}$, $Z = 6 \text{ m}$) (location
- 949 in Fig. 5). The measured blank $^{10}\text{Be}/^9\text{Be}$ ratio is $(4.40 \pm 1.97) \times 10^{-16}$. Age interpretations are presented
- 950 in Fig. 8.
- 951
- 952 3) $^{26}\text{Al}/^{10}\text{Be}$ raw data and burial durations for the samples of the borehole GBEC5. The Matlab© code and
- 953 the parameters summarized in (Blard et al., 2019) were used to compute the $^{26}\text{Al}/^{10}\text{Be}$ burial ages, with a
- 954 catchment mean altitude of pre-burial exposure of 926 m, similar to present-day. Note that ^{10}Be
- 955 concentration has been measured both at ASTER and PRIME Lab AMS. ^9Be (at) is the amount of added
- 956 carrier, while ^{27}Al (at) corresponds to the sum of the natural ^{27}Al (at) measured in the sample and the
- 957 amount of added carrier. Blank $^{10}\text{Be}/^9\text{Be}$ ratio for ASTER measurements is $(1.94 \pm 0.54) \times 10^{-15}$. Blank
- 958 $^{10}\text{Be}/^9\text{Be}$ ratio for PRIME lab measurements is $(0.65 \pm 0.75) \times 10^{-15}$. Blank $^{26}\text{Al}/^{27}\text{Al}$ ratio is (1.45 ± 1.39)

959 x 10⁻¹⁵. The interlaboratory comparison of ¹⁰Be concentrations shows an agreement within uncertainties.
960 **Bold data** corresponds to ²⁶Al/¹⁰Be with the lowest uncertainties and are the age retained in our
961 interpretations. *Italic data* correspond to ratio with higher uncertainties.

962

963 4) Synthesis of published OSL/IRSL data in the Golo alluvial plain.

964

Figure 1

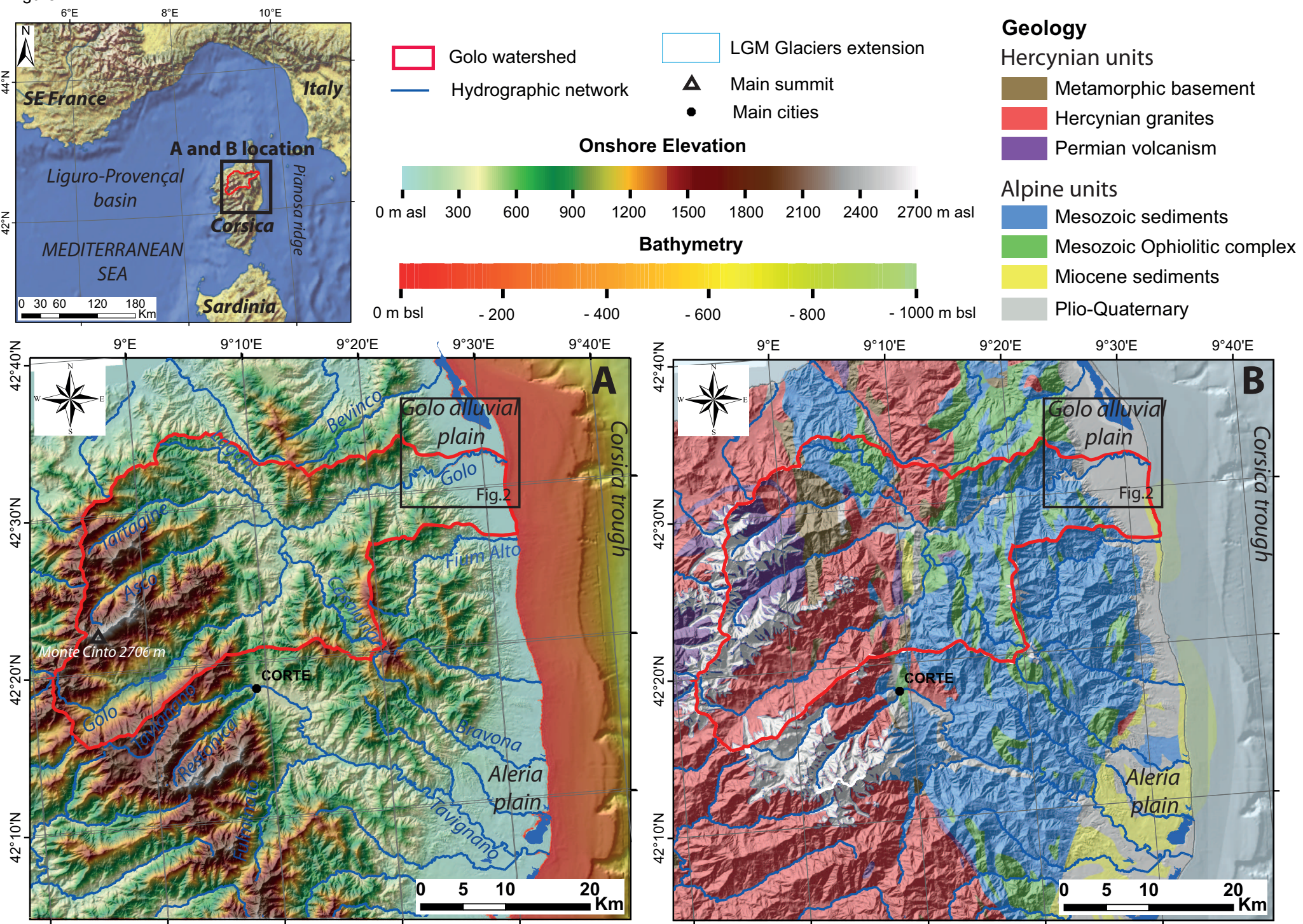
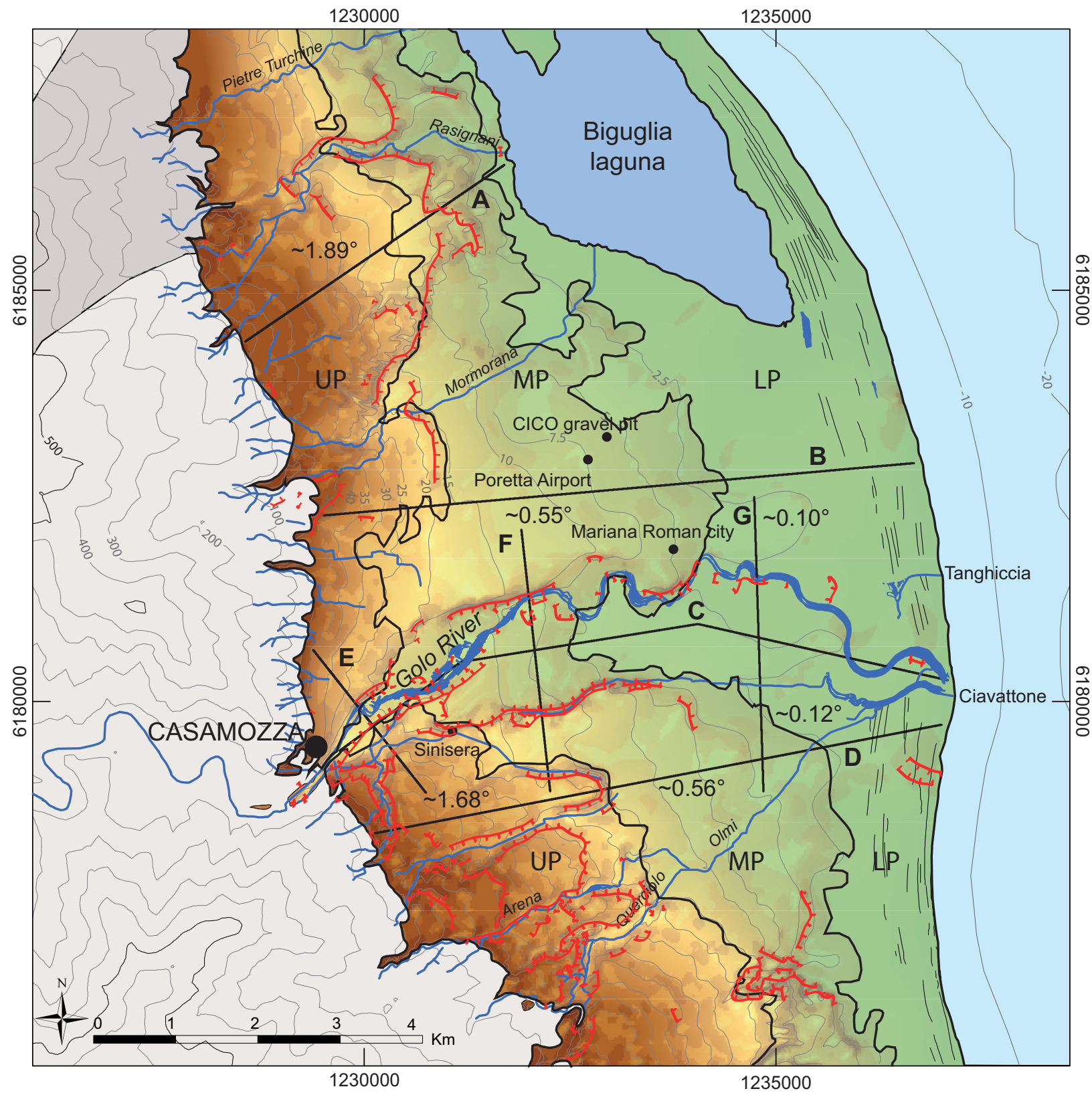


Figure2



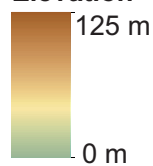
Bedrock domain

- Phyllides
- Ophiolites

Hydrology

- Hydrographic network

Elevation



Geomorphological features

- Beach ridges
- Escarpments

Morphologic area

- UP: Upper Plain
- MP: Middle Plain
- LP: Lower Plain

Figure3

- Colluvium
- Ferralsol and Luvisol (Fw; Fx)
- Reddish Brunisol (Fy1)
- Brunisol (Fy2)
- Row (Fz) and Typical (Fy3) Fluvisol
- Coastal soils (Mz)

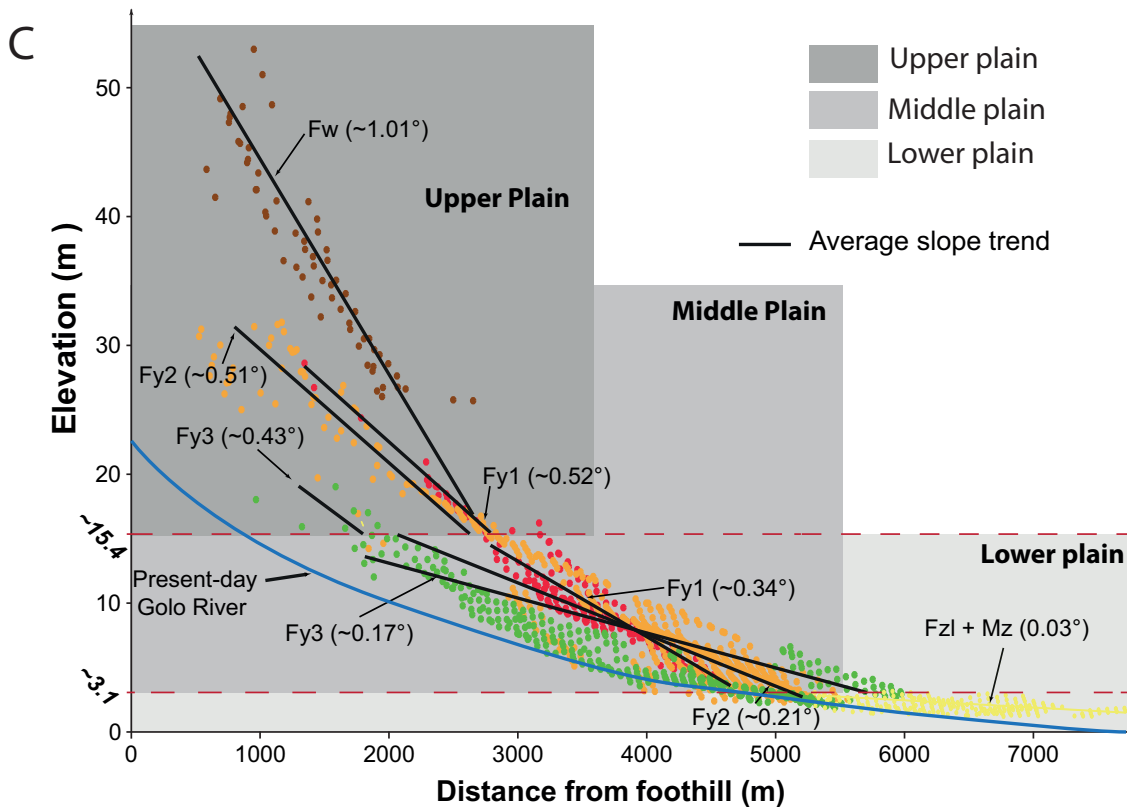
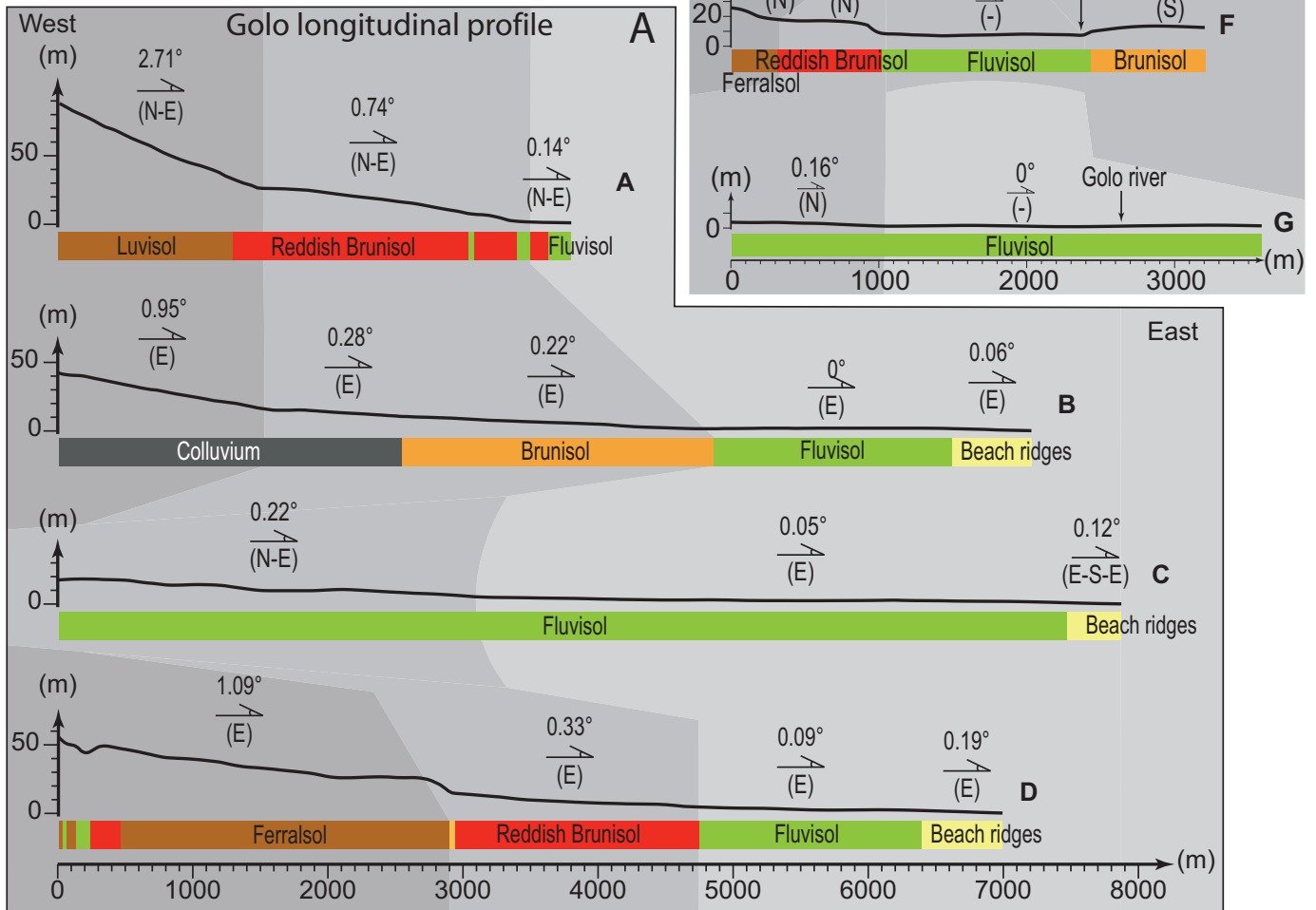
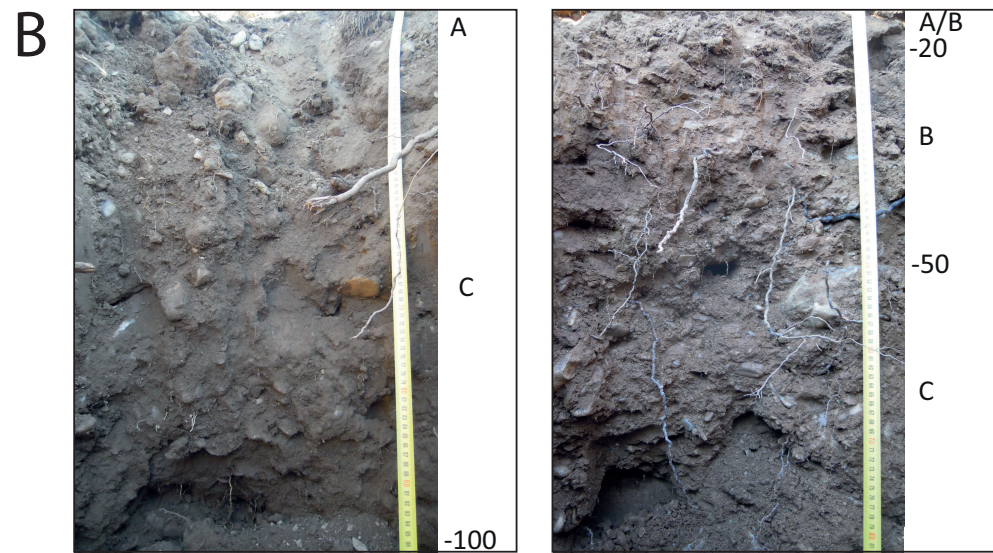
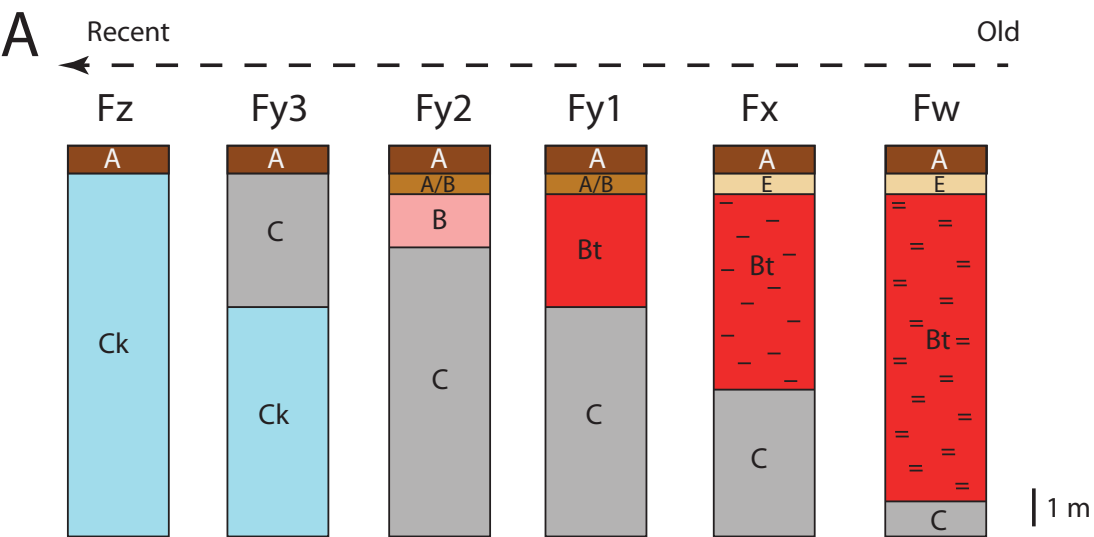
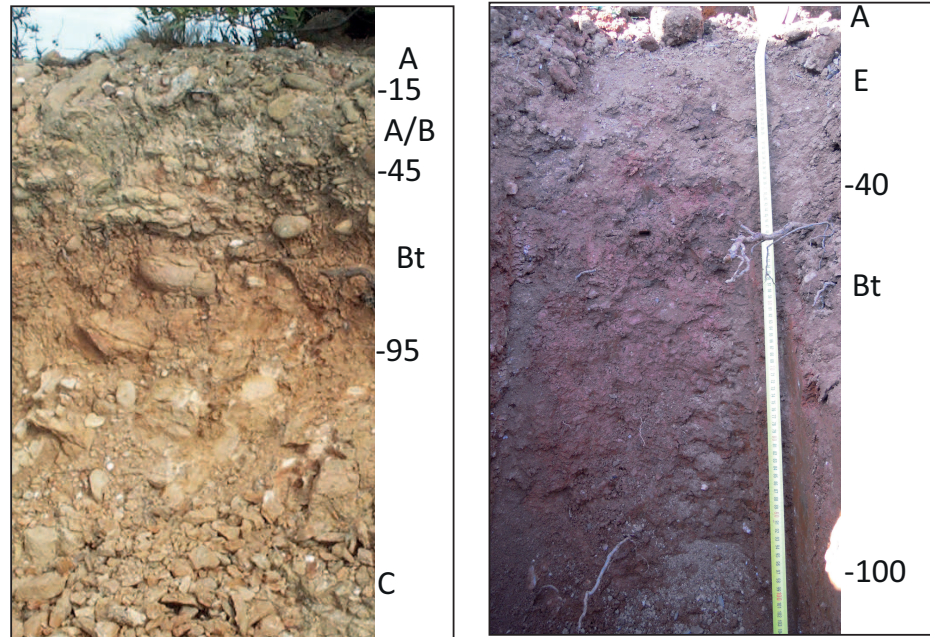


Figure 4



- A** Humic surface horizon, sandy loam to loam (0 to 20-30 cm).
- A/B** Transition horizon between A and Bw, sandy loam to loam (20-30 to 50-60 cm).
- E** Eluviated horizon depleted in iron, organic matter and sometimes clay (20-30 to 50-60 cm).
- B** Weathering horizon slightly enriched in clay (beginning of leaching and rubbing) (50-60 to 80-90 cm).
- Bt** Horizon enriched in clay, often fersiallitic, lloam, quite thick (at least 1 m).
- Bt-** Horizon very enriched in clay, sometimes hydromorphic, very often fersiallitic, loam to clay loam, thick (at least 2 m).
- Bt=** Horizon very enriched in clay, mostly hydromorphic, otherwise fersiallitic, clay loam, very thick (at least 5 m).
- Ck** Braided alluvial material, sometimes partly carbonated in some very recent formations.



C

Process	Fz	Fy3	Fy2	Fy1	Fx	Fw
Decarbonation		+++	Decarbonated soils			
Acidification			+	++	+++	++++
Browning	(+)	++	+++	+	+	+
Reddening			(+)	++	+++	++
Leaching			+	++	+++	++++
Hydromorphy				(+)	+	++
Degradation					(+)	+
Weathering degree			(+)	+	++	+++
Deep weathering			+	++	++/+++	+++

Fy1

Fw

Figure5

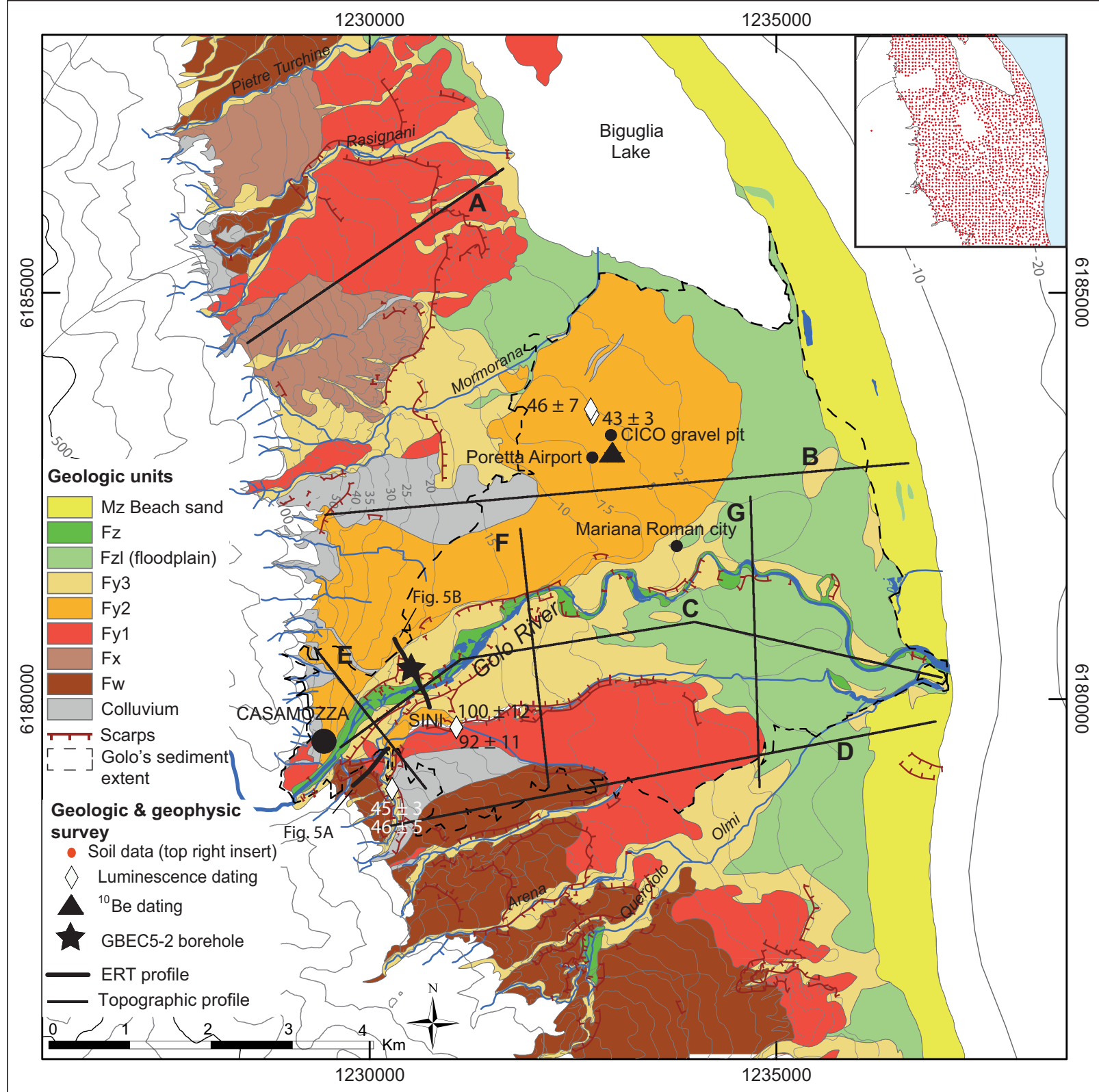


Figure 6

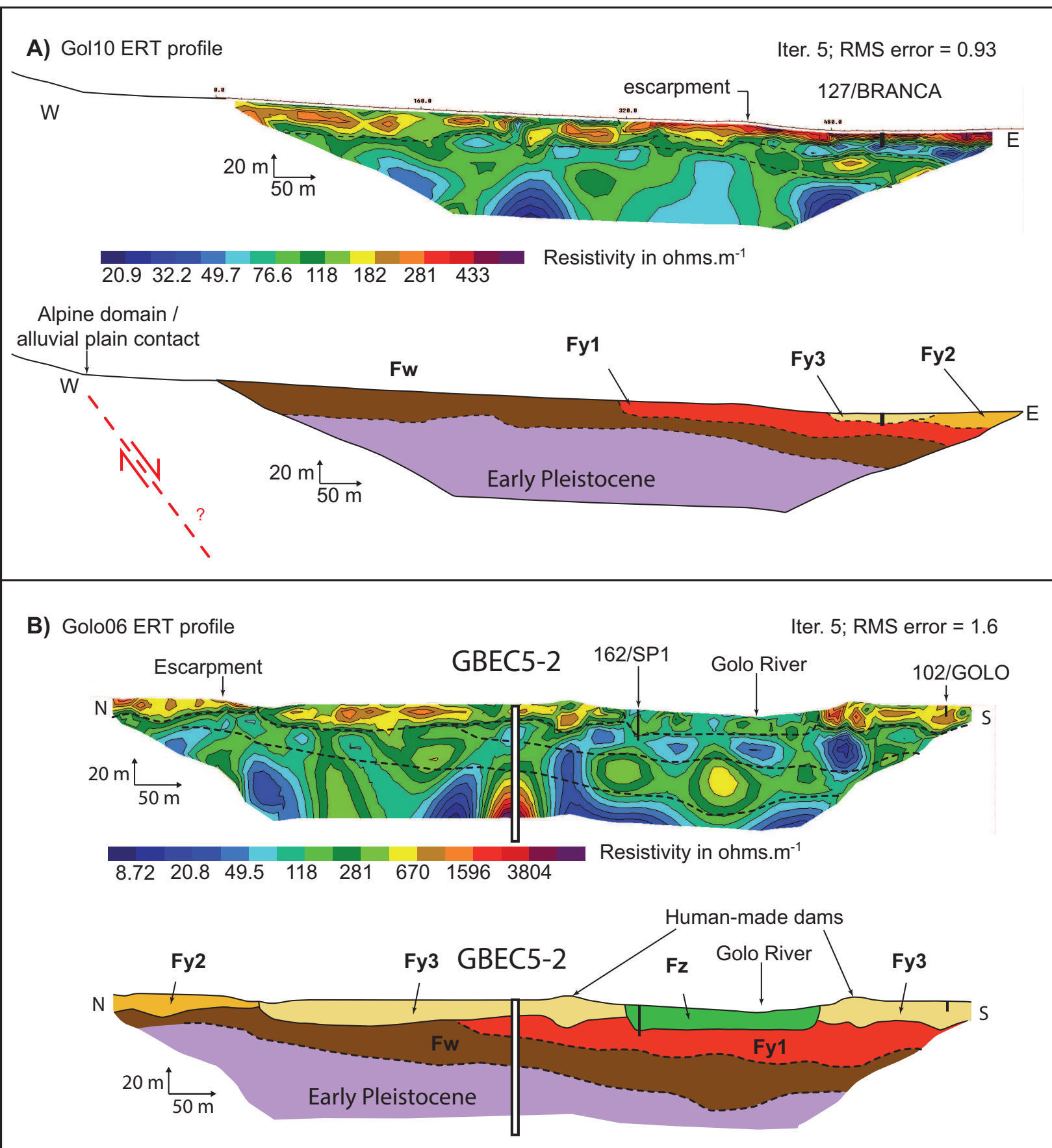


Figure 7

GBEC 5-2 : Synthetic log

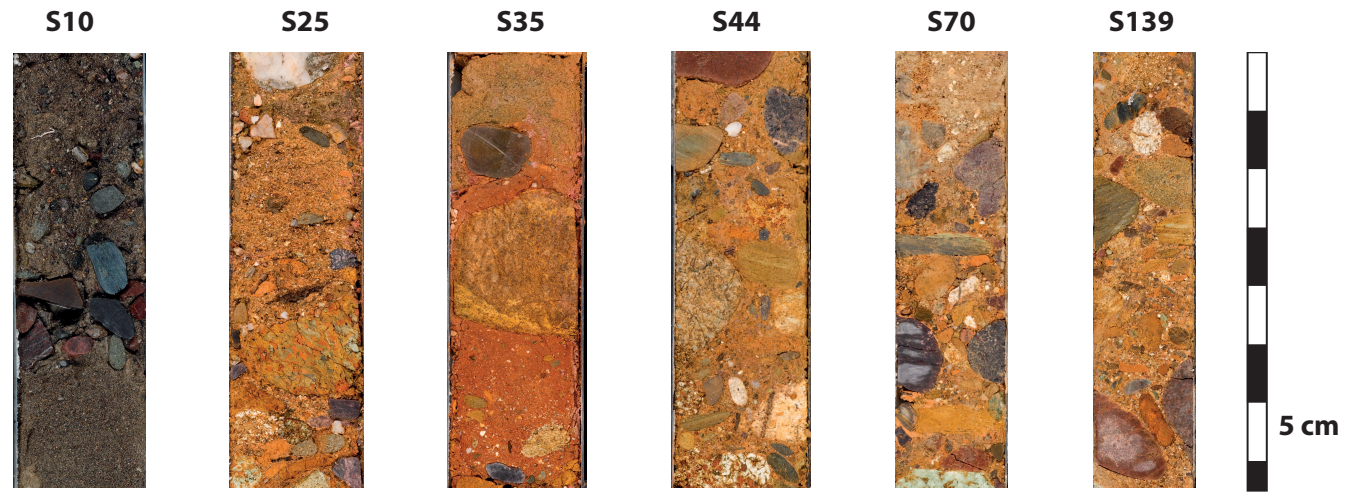
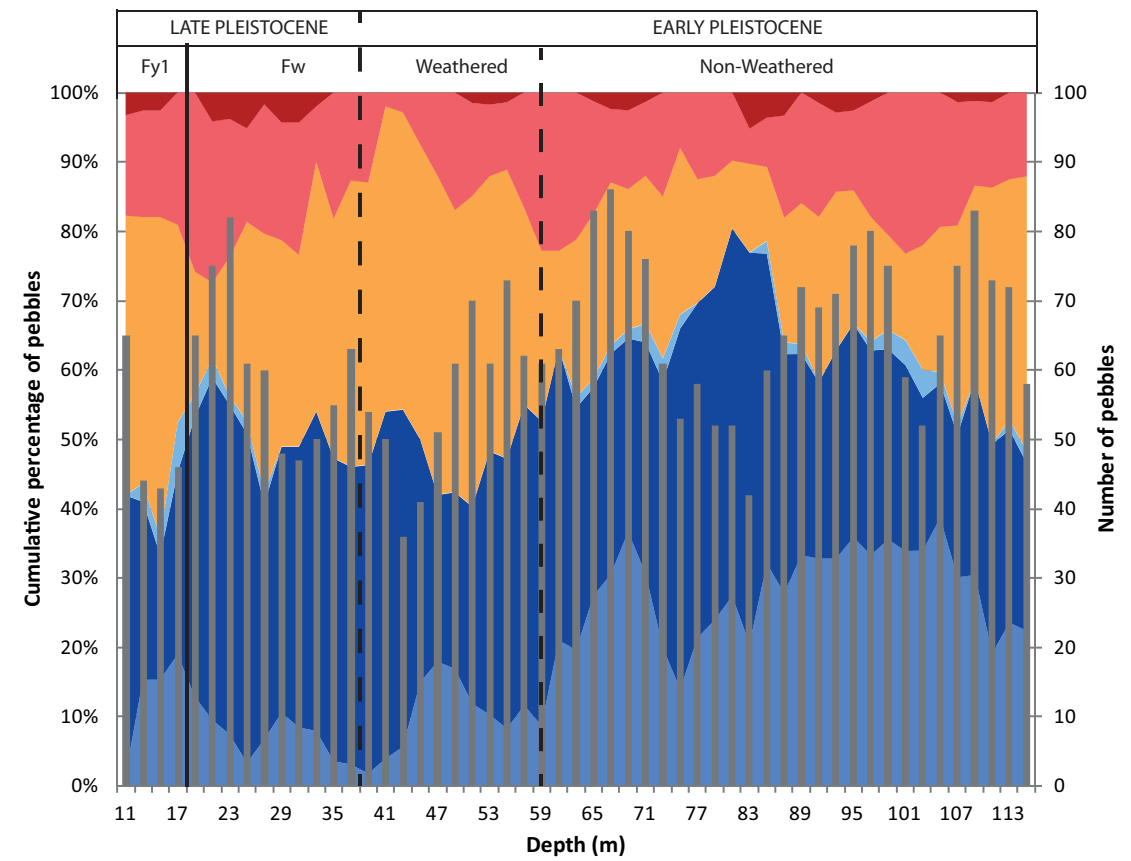
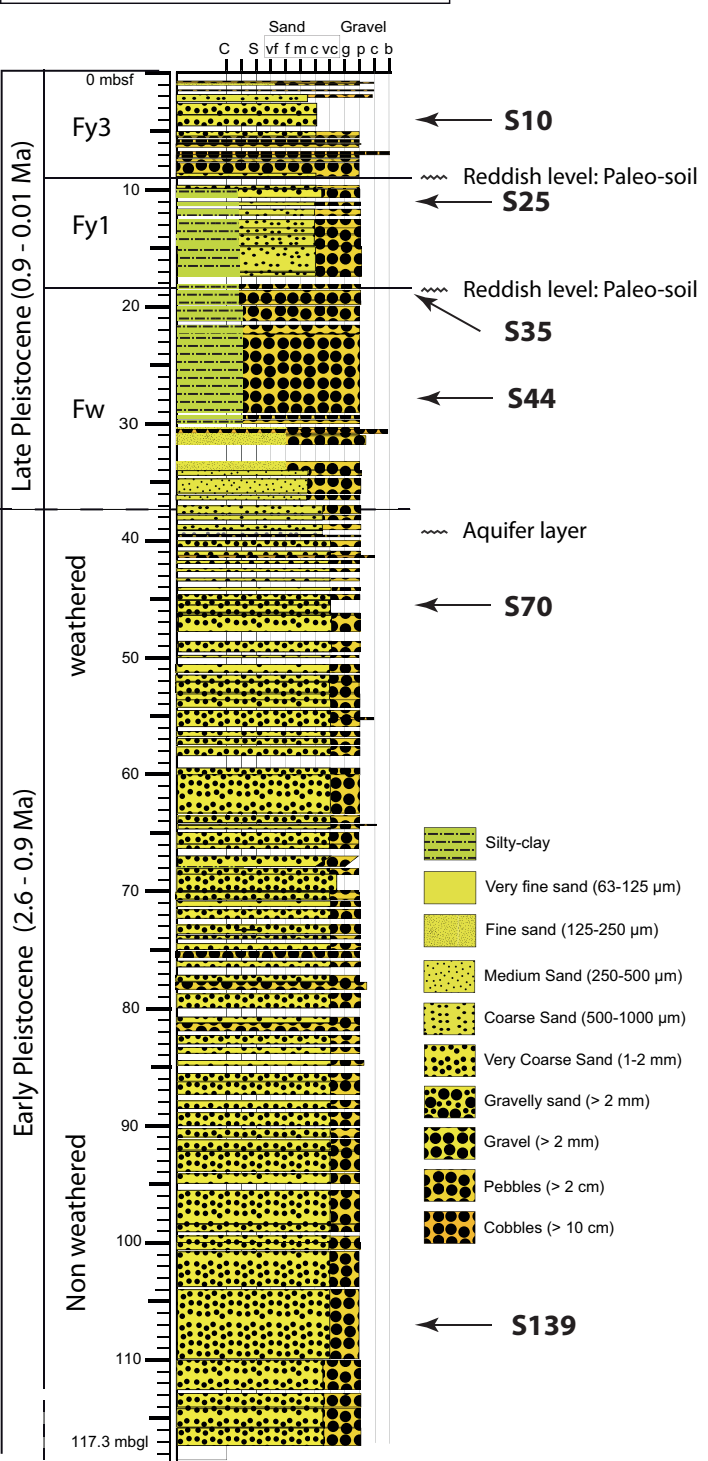


Figure 8

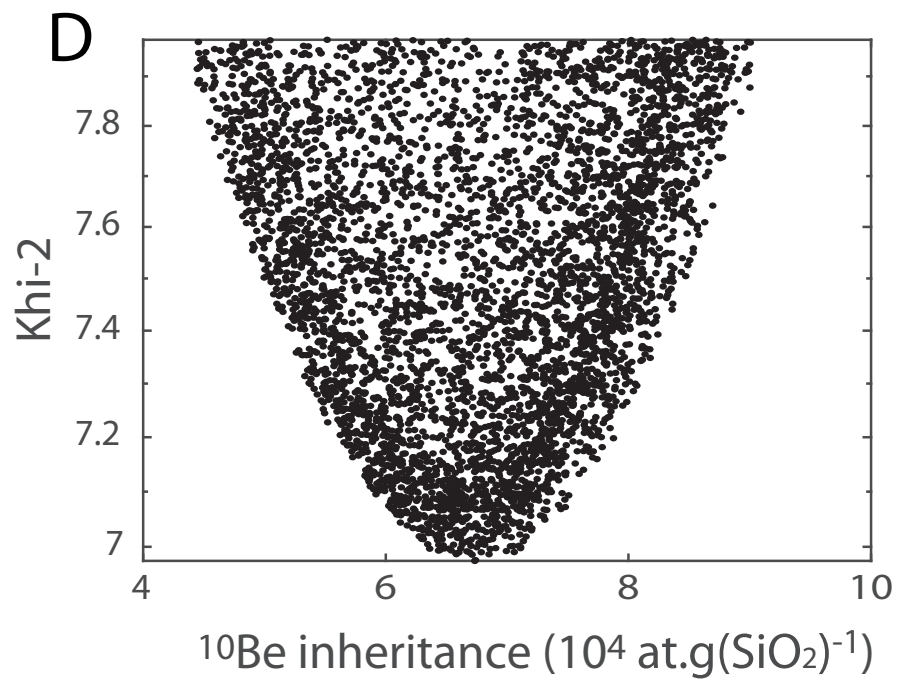
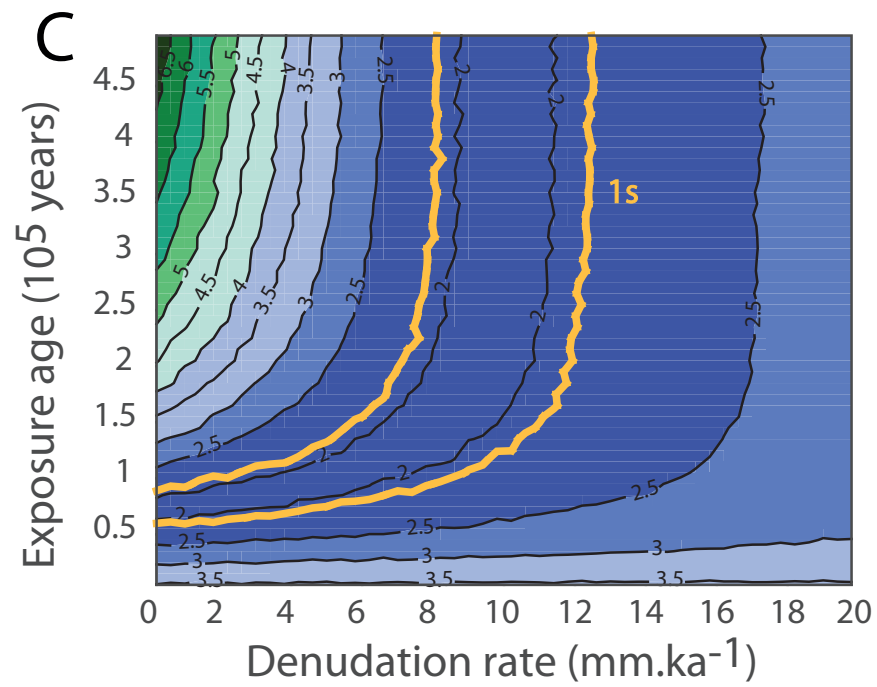
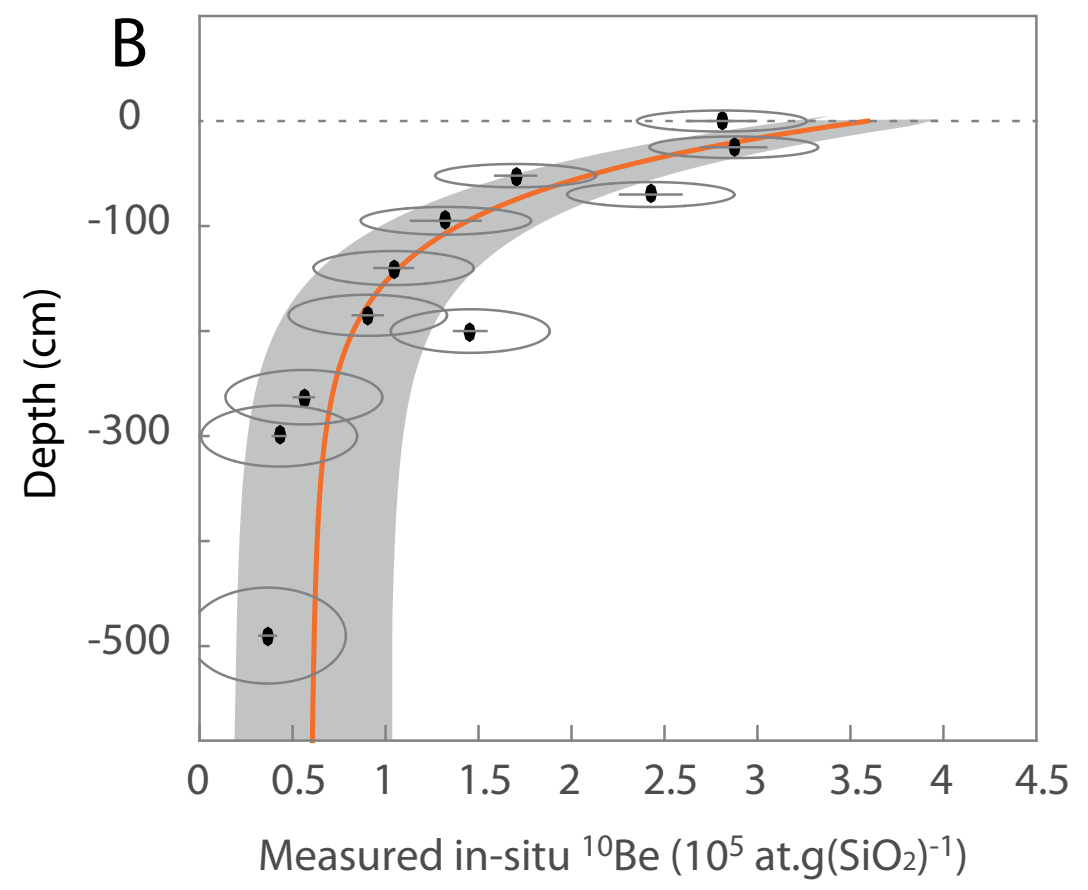
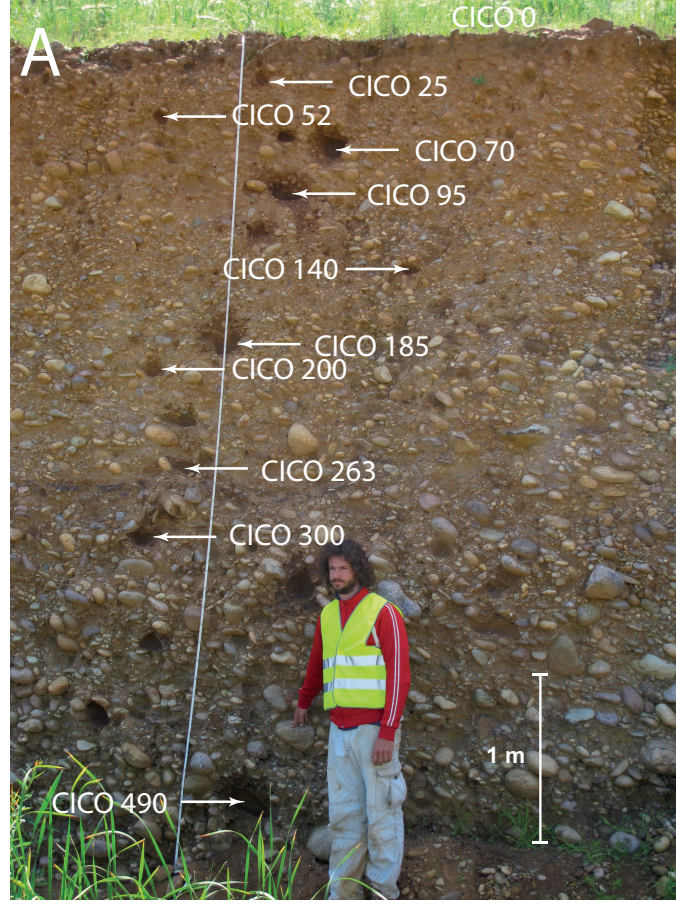


Figure9

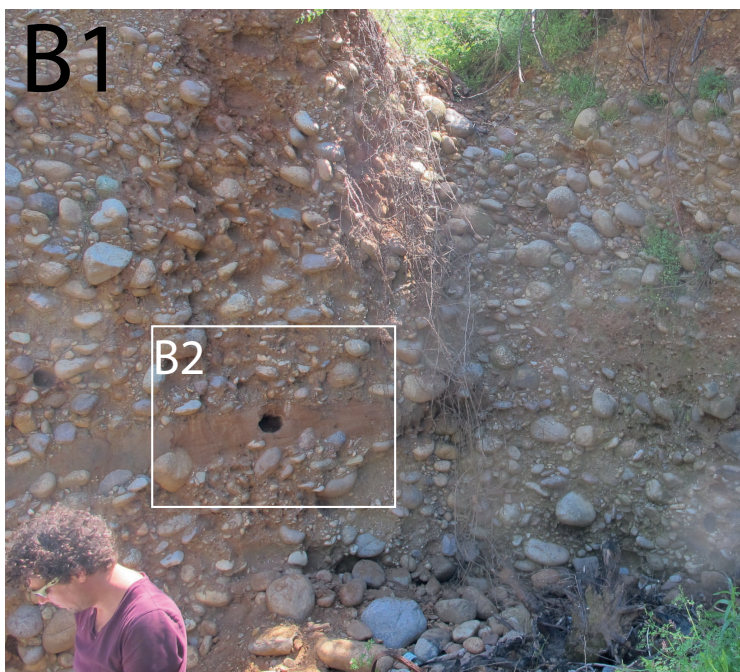
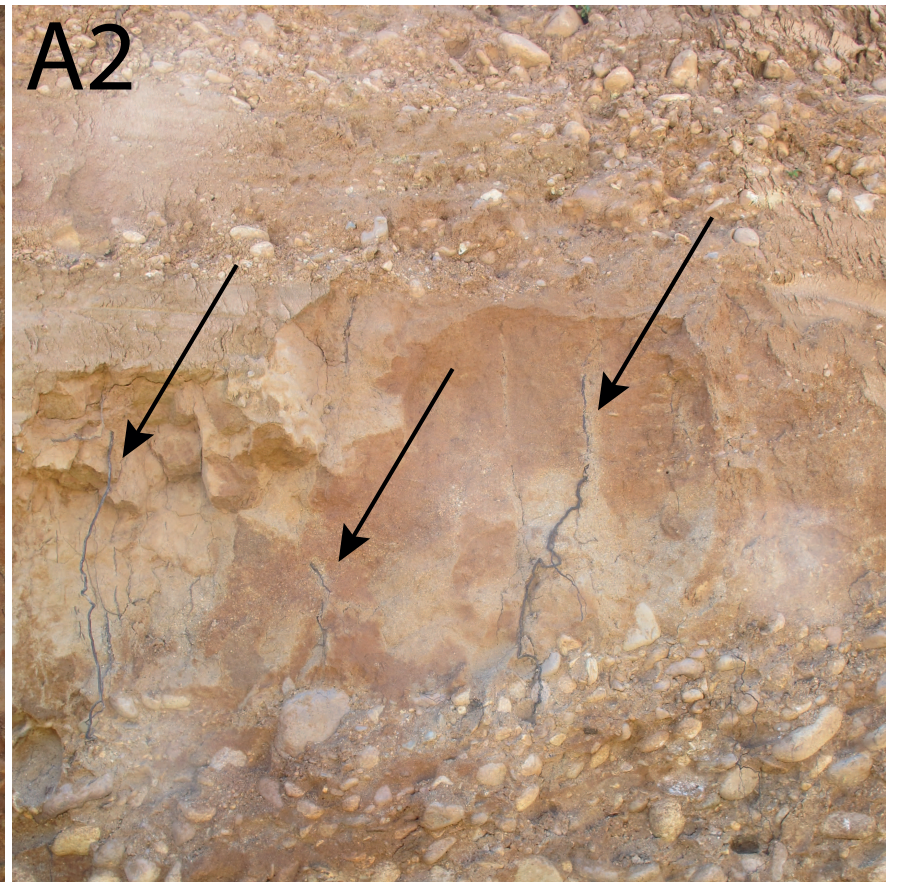
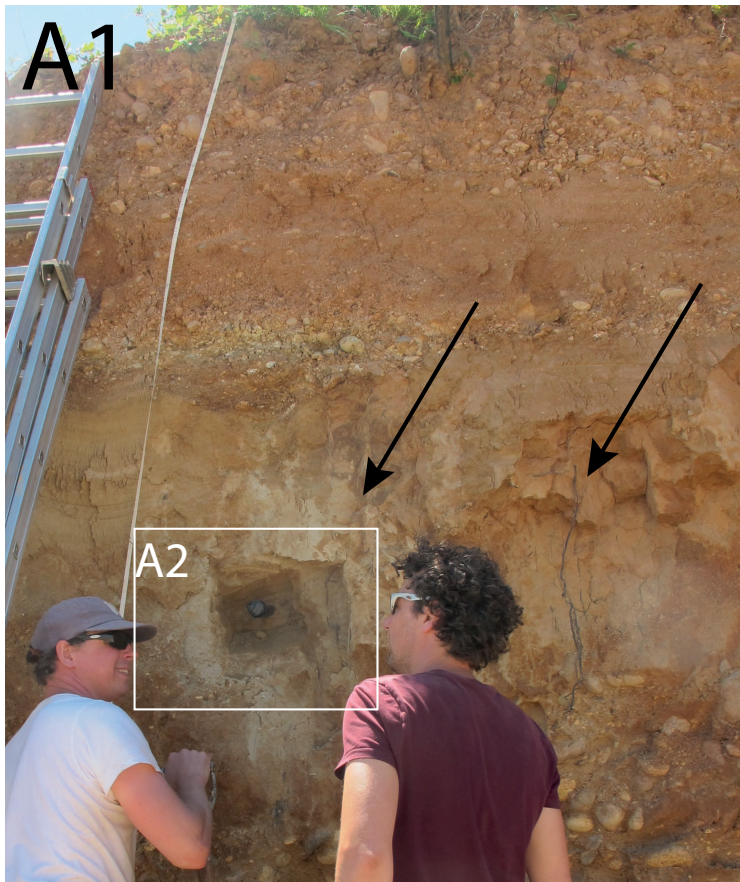


Figure10

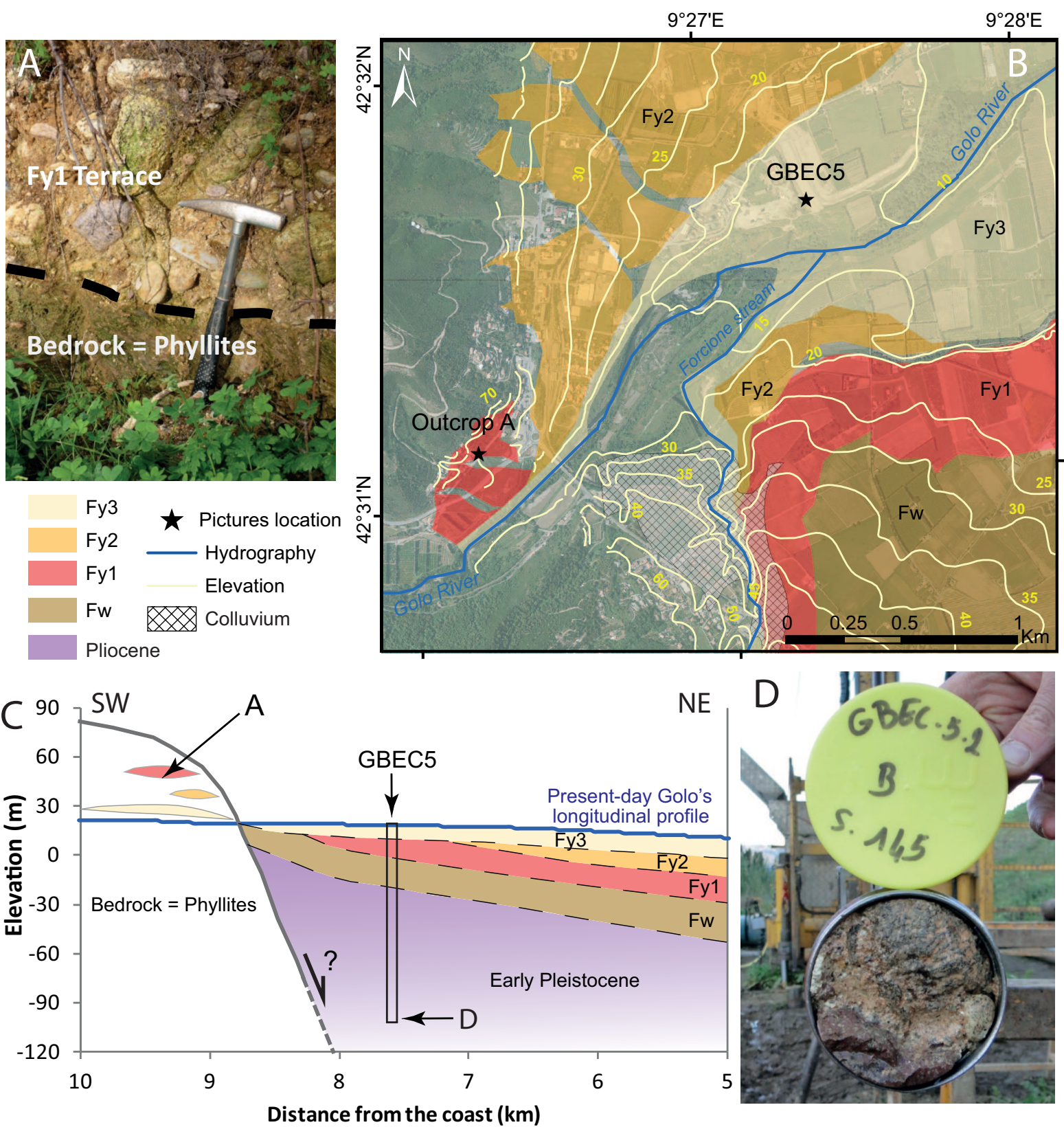


Table1

Geologic Map Unit (BRGM)	Alternative nomenclature	Type of soil associated	Electrical Resistivity ($\Omega.m^{-1}$)		
				Conchon, 1989	Somme
Fz	N7	Row Fluvisol	120-250	1	
Fy3	N6	Typical Fluvisol	300-800	2	
Fy2	N5	Brown Soil	350-800	3	
Fy1	N4	Reddish Brown Soil	240-600	4	
Fx	N3	Luvisol	-	6	
Fw	N2	Ferralsol	80-350	8	
Fv	N1	-	10-80	10	

Table2

Sample name	Depth (cm)	Mass of dissolved Quartz (g)	$^{10}\text{Be}/^9\text{Be}$ ($\times 10^{-14}$)	^9Be ($\times 10^{19}$ at)	^{10}Be $\times 10^4$ at.g(SiO_2) $^{-1}$
CICO 0	0	20.13	13.173 \pm 0.592	2.022	28.09 \pm 1.82
CICO 25	25	14.31	9.573 \pm 0.371	2.024	28.73 \pm 1.75
CICO 52	52	21.07	8.395 \pm 0.383	2.010	17.00 \pm 1.10
CICO 70	70	7.87	4.444 \pm 0.219	2.031	24.27 \pm 1.65
CICO 95	95	20.01	6.169 \pm 0.818	2.027	13.25 \pm 1.87
CICO 140	140	20.43	4.951 \pm 0.428	2.033	10.43 \pm 1.03
CICO 185	185	20.38	4.300 \pm 0.347	2.025	9.04 \pm 0.81
CICO 200	200	20.61	6.879 \pm 0.256	2.056	14.56 \pm 0.87
CICO 263	263	20.32	2.656 \pm 0.222	2.034	5.61 \pm 0.54
CICO 300	300	20.20	2.009 \pm 0.281	2.042	4.27 \pm 0.34
CICO 490	490	20.28	1.729 \pm 0.207	2.042	3.66 \pm 0.45

Table3

Name	GBEC5-2 Depth (m)	Mass of dissolved quartz (g)	$^{10}\text{Be}/^9\text{Be}$ Ratio ($\times 10^{15}$)	^9Be ($\times 10^{19}$ at)	^{10}Be $\times 10^4$ at.g $^{-1}$ (SiO $_2$)	AMS	$^{26}\text{Al}/^{27}\text{Al}$ Ratio ($\times 10^{15}$)	^{27}Al ($\times 10^{19}$ at)	^{26}Al $\times 10^4$ at.g(SiO $_2$) $^{-1}$	$^{26}\text{Al}/^{10}\text{Be}$ ratio	Burial duration (Ma)
B5 S59	37.8	9.888	23.410 \pm 2.268	2.310	4.89 \pm 0.47	ASTER	10.74 \pm 2.88	2.243	10.75 \pm 3.32	2.198 \pm 0.711	2.45 \pm 0.73
<i>B5 S59</i>	<i>37.8</i>	<i>3.119</i>	<i>7.950 \pm 1.710</i>	<i>1.711</i>	<i>4.00 \pm 1.02</i>	<i>PRIME Lab</i>	<i>10.74 \pm 2.88</i>	<i>2.243</i>	<i>10.75 \pm 3.32</i>	<i>2.689 \pm 1.077</i>	<i>1.94 \pm 0.89</i>
<i>B5 S145</i>	<i>116.5</i>	<i>11.144</i>	<i>16.6 \pm 2.227</i>	<i>2.310</i>	<i>2.93 \pm 0.39</i>	<i>ASTER</i>	<i>7.391 \pm 1.965</i>	<i>2.213</i>	<i>7.43 \pm 2.46</i>	<i>2.535 \pm 0.906</i>	<i>2.15 \pm 0.80</i>
B5 S145	116.5	3.090	7.839 \pm 1.793	1.711	3.97 \pm 1.07	PRIME Lab	7.391 \pm 1.965	2.213	7.43 \pm 2.46	1.870 \pm 0.799	2.74 \pm 0.95

Table4

Sample Name	Lat. (N)	Long. (E)	Terrace	Depth (m)	Method	Absolute age	Reference
NCL-5212119	42°33'15.468"	9°29'05.874"	Fy2-CICO	2.00	pIRIR ₂₉₀	43 ± 4 ka	Forzoni et al., 2011
NCL-5212120	42°33'17.581"	9°29'05.025"	Fy2-CICO	2.10	pIRIR ₂₉₀	46 ± 7 ka	Forzoni et al., 2011
NCL-5212118	42°31'15.269"	9°27'38.805"	Fy1-SINI	4.10	pIRIR ₂₉₀	92 ± 11 ka	Forzoni et al., 2011
NCL-5212116	42°31'15.269"	9°27'38.805"	Fy1-SINI	4.30	pIRIR ₂₉₀	100 ± 12 ka	Forzoni et al., 2011
Golo 6A	42°30'52.759"	9°27'01.337"	Fw	2.00	OSL	45 ± 3 ka	Somme et al., 2011
Golo 6B	42°30'52.759"	9°27'01.337"	Fw	2.00	OSL	76 ± 5 ka	Somme et al., 2011



Dr. Stéphane Molliex
Laboratoire Géosciences Océan
IUEM, UMR 6538
Place N. Copernic
F-29280 Plouzané
France
Tel: +33 2 98 8910 04
Email: smolliex@gmail.com

Editor of *Quaternary Geochronology*

Subject: Submission of a manuscript to "*Quaternary Geochronology*"

Dear Editor,

We declare that we have no conflict of interest in the research called "*Revisiting extent and chronology of the Golo River alluvial plain deposits (NE Corsica, France).*" by S. Molliex and co-authors that we submit for consideration of publication in *Quaternary Geochronology*. Please note nevertheless that an associate editor of *Quaternary Geochronology* (P.-H. Blard) is co-author of this work.

Best Regards,

Dr. Stéphane Molliex on behalf of all co-authors